AD NUMBER

ADB230946

NEW LIMITATION CHANGE

TO

Approved for public release, distribution unlimited

FROM

Distribution authorized to U.S. Gov't. agencies only; Specific Authority; 31 Oct 97. Other requests shall be referred to Commander, U.S. Army Medical Research and Materiel Command, Attn: MCMR-RMI-S, Fort Detrick, Frederick, MD 21702-5012.

AUTHORITY

USAMRMC ltr, 4 Dec 2002

AD_____

CONTRACT NUMBER DAMD17-97-C-7016

TITLE: Development of Reactive Topical Skin Protectants Against Sulfur Mustard and Nerve Agents

PRINCIPAL INVESTIGATOR: Kenneth Klabunde, Ph.D.

CONTRACTING ORGANIZATION: Nantek, Incorporated
Manhattan, Kansas 66502

REPORT DATE: June 1997

TYPE OF REPORT: Final - Phase I

PREPARED FOR: Commander
U.S. Army Medical Research and Materiel Command
Fort Detrick, Frederick, Maryland 21702-5012

REPORT DOCUMENTATION PAGE

Form Approved
OMB No. 0704-0188

1. AGENCY USE ONLY *(Leave blank)*	2. REPORT DATE	3. REPORT TYPE AND DATES COVERED
	June 1997	Final-Phase I (15 Nov 96 - 14 May 97)

4. TITLE AND SUBTITLE
Development of Reactive Topical Skin Protectants Aganist Sulfur Mustard and Nerve Agents

5. FUNDING NUMBERS
DAMD17-97-C-7016

6. AUTHOR(S)
Kenneth Klabunde, Ph.D.

7. PERFORMING ORGANIZATION NAME(S) AND ADDRESS(ES)
Nantek, Incorporated
Manhattan, Kansas 66502

8. PERFORMING ORGANIZATION REPORT NUMBER

9. SPONSORING/MONITORING AGENCY NAME(S) AND ADDRESS(ES)
Commander
U.S. Army Medical Research and Materiel Command
Fort Detrick, Frederick, Maryland 21702-5012

10. SPONSORING/MONITORING AGENCY REPORT NUMBER

11. SUPPLEMENTARY NOTES

12a. DISTRIBUTION / AVAILABILITY STATEMENT
31 OCT 1997
Distribution authorized to U.S. Government agencies only (specific authority). Other requests for this document shall be referred to Commander, U.S. Army Medical Research and Materiel Command, ATTN: MCMR-RMI-S, Fort Detrick, Frederick, Maryland 21702-5012.

12b. DISTRIBUTION CODE

13. ABSTRACT *(Maximum 200*

The purpose of the Phase I Research was to investigate the feasibility of using Nantek's unique reactive nanoparticle (RNP) adsorbents as the active ingredient in a skin cream system for the protection against exposure to sulfur mustard and nerve agents. The scope of the work included: (1) study of mimic reactions with a broad array of adsorbents; (2) new adsorbent formulation development; (3) adsorbent-cream compatibility studies; (4) prototype skin system testing; and (5) reaction studies with actual nerve and mustard agents.

Overall technical feasibility was established with the following major findings include: (1) RNP adsorbents are highly reactive and in some instances nearly instantaneously destroyed VX and its mimics; (2) actual evidence of decomposition and not merely absorption was observed; (3) HD and its mimics are partially decomposed by the RNP adsorbents suggesting the need for further optimization of the adsorbent formulations in Phase II; and (4) the most efficient RNP adsorbents demonstrated chemical compatibility and reactivity when embedded in the selected base cream.

14. SUBJECT TERMS
Adsorption; destruction; chemical agents; skin protection; nanoparticles; ultrafine; metal oxides; detoxification

15. NUMBER OF PAGES
59

16. PRICE CODE

17. SECURITY CLASSIFICATION OF REPORT	18. SECURITY CLASSIFICATION OF THIS PAGE	19. SECURITY CLASSIFICATION OF ABSTRACT	20. LIMITATION OF ABSTRACT
Unclassified	Unclassified	Unclassified	Limited

FOREWORD

Opinions, interpretations, conclusions and recommendations are those of the author and are not necessarily endorsed by the U.S. Army.

____ Where copyrighted material is quoted, permission has been obtained to use such material.

____ Where material from documents designated for limited distribution is quoted, permission has been obtained to use the material.

____ Citations of commercial organizations and trade names in this report do not constitute an official Department of Army endorsement or approval of the products or services of these organizations.

____ In conducting research using animals, the investigator(s) adhered to the "Guide for the Care and Use of Laboratory Animals," prepared by the Committee on Care and Use of Laboratory Animals of the Institute of Laboratory Resources, National Research Council (NIH Publication No. 86-23, Revised 1985).

____ For the protection of human subjects, the investigator(s) adhered to policies of applicable Federal Law 45 CFR 46.

____ In conducting research utilizing recombinant DNA technology, the investigator(s) adhered to current guidelines promulgated by the National Institutes of Health.

____ In the conduct of research utilizing recombinant DNA, the investigator(s) adhered to the NIH Guidelines for Research Involving Recombinant DNA Molecules.

____ In the conduct of research involving hazardous organisms, the investigator(s) adhered to the CDC-NIH Guide for Biosafety in Microbiological and Biomedical Laboratories.

Kenneth J. Klabnik June 12 1997

PI - Signature Date

TABLE OF CONTENTS

1.0 INTRODUCTION

1.1 Introduction to Nantek's Destructive Adsorption Technology

The need for military personnel protective systems capable of neutralizing highly toxic substances such as the nerve agents GA, GB, BD, and VX has been identified as a significant problem facing the Department of Defense.[1-25] For the specific application addressed in this proposal, reactive adsorbent materials could be mixed into a base cream to provide protection for skin in the event of exposure to such highly toxic substances. Other counter measure or protective uses for the adsorbents could include air purification, personnel ventilation systems, and wide-area surface decontamination.

Significant work has been conducted at Kansas State University under the leadership of University Distinguished Professor Dr. Kenneth J. Klabunde resulting in the discovery of unique nanoparticle materials exhibiting extraordinary abilities to destroy highly toxic substances such as nerve agents, PCBs, and insecticides.[21-25] Much of the basic research in nanoparticle synthesis and reactive chemistry has been funded by a variety of federal grant sources including the Department of Army. From this basic research focusing on the synthesis, characterization, and reaction chemistry of a broad range of nanoparticle materials, several patents are pending on the unique nanoparticles and the underlying Destructive Adsorption Technology (DAT).

Essentially, the research conducted prior to the Phase I research had demonstrated the ability of the unique nanoparticles to both adsorb and destroy hazardous compounds. Initial work focused on the use of DAT as an alternative to high temperature incineration for the bulk treatment of organophosphorus compounds, chlorinated hydrocarbons, PCBs, insecticides and other similar hazardous substances. On a laboratory scale, special metal oxide nanoparticles destructively adsorbed mimics of nerve gases including paraoxon, one-armed mustard, and DMMP as well as CCl_4, a fairly stable compound. Prior to the Phase I Research, laboratory results strongly suggested that the nanoparticles indeed react with these substances at room temperature thus opening the application to personal and building ventilation systems, protective skin products, and wide-area surface decontamination.

The nanoparticles seem to provide a clear advantage over other competing decontamination technologies such as activated carbon adsorbents and other highly caustic solutions. Other liquid decontaminates used primarily for surface decontamination, such as DS2, Oxone, and ethanol-NaOH-ammonia solutions[26], are highly toxic for skin exposure and would not be compatible with the proposed base skin cream. Activated carbon, a possible solid adsorbent, has the disadvantages of:

(1) Carbon does not destroy the toxic chemical but merely "holds it" by weak adsorption forces;

(2) Inorganic pollutants such as hydrogen cyanide, cyanogen chloride, and acid gases are not adsorbed well by activated carbon, and

(3) Clean-up and disposal of the contaminated carbon is difficult since the hazardous material is believed to be only adsorbed but still highly toxic.

Caustic sorbents are obviously unsuitable for this application posing a significant hazard for humans. In fact, the solutions used for such purposes are so highly caustic that they corrode metals, paint and wood.

Thus, new materials or adsorbents offering rapid kinetics yet suitable from a safety and cost standpoint need to be developed that can protect skin from exposure to highly toxic nerve agents when combined with a suitable barrier base cream. The unique nanoparticle adsorbents under development by Nantek, Inc., offer significant potential in satisfying these difficult technical and economic challenges.

1.2. Purpose of the Phase I Research

The main objective of the Phase I Research was to demonstrate the chemical feasibility of nanoscale destructive adsorbents as the active ingredient for a topical skin protectant against mustard and nerve agents. To meet this objective four specific tasks were undertaken. First, a broad array of nanoparticles were fabricated and tested under ambient conditions to identify the likely best alternatives for the topical

skin protectant application. Second, compatibility of the nanoparticles within the base cream was studied focusing primarily on suspension stability and chemical compatibility of the adsorbents with other components in the base cream. Third, the performance of the destructive adsorbents were confirmed with real military agents through limited laboratory tests conducted in cooperation with the Midwest Research Institute. Finally, a prototype reactive topical skin protectant system was formulated and the reaction efficacy of the adsorbents was evaluated on a preliminary basis in the presence of the base cream ingredients.

2.0 PHASE I RESEARCH RESULTS

2.1 General Approach and Overview of Nantek's Unique Nanoparticle Synthesis Schemes

Several unique nanoparticles were developed during the Phase I Research that were believed to be possible candidates for the skin cream protectant system. These included oxides of magnesium, titanium, calcium, zinc, nickel, and copper, magnesium and calcium hydroxides, and composite samples consisting of transition metal coated nanoparticles. The following approach was taken for sample preparation and analysis. Commercially available products were first tested for paraoxon adsorption. If the results of such testing exhibited even modest levels of reactivity, Nantek's standard particle synthesis approaches, either conventionally- or autoclave-prepared, were attempted. The resulting nanoparticles were then studied for enhanced reactivity and destructive capacity.

As a review, autoclave-prepared (AP) samples generally involve the addition of toluene to a metal-methanol solution. Upon autoclave treatment, the solution is converted to a gel-like metal-hydroxide solution. After the hypercritical drying step, a high temperature dehydration step is required. This is done under a vacuum, but can also be accomplished by a fast flow of hot nitrogen gas.

Conversely, the lower surface area, conventionally prepared (CP) samples do not require the hypercritical drying step or the addition of solvents. Commercial metal oxides are boiled in distilled water. The resulting slurry is filtered and dried to form metal-hydroxide crystals. These crystals undergo a high temperature dehydration step to yield the fine, CP powders.

For composite materials such as iron coated, autoclave prepared calcium oxide (Fe/AP-CaO), the AP powder is treated with a $Fe(acac)_3$ solution in pure THF. The mixture is stirred overnight at room temperate allowing $Fe(acac)_3$ to adsorb onto the MgO surface. After filtering and washing with pure, dry THF, the sample is dried and heat treated under vacuum conditions. The resulting composite essentially has a monolayer of iron oxide coating the high surface area metal oxide nanocrystals.

Preparation of high surface area zinc oxide proved to be a challenge during the Phase I effort since Nantek's standard processes failed to yield high surface area zinc oxide powders. Note the standard AP-synthesis method includes adding toluene to a metal/methanol mixture. However, zinc metal does not react with methanol to produce zinc methoxide. Two sol-gel synthesis approaches were then attempted for the preparation of zinc oxide to obviate the traditional methanol step. First, zinc acetate was dissolved in absolute ethanol, and part of the ethanol was distilled off. In this step acetate groups were partially replaced by ethoxide groups. Then LiOH H_2O was added to hydrolyze the ethoxide, and concentrated by removing the solvent. The product was then dried in a dessicator for a few days. The XRD spectra (shown in Figure 1) did not agree with either zinc oxide, zinc hydroxide, or zinc acetate reference spectra. The surface area of the product was 7 m^2/g compared to an area of 14.5 m^2/g for conventionally prepared material.

The second method used was starting with zinc acetate that was dissolved in 2-methoxyethanol and then added to diethylamine. The XRD spectrum matched exactly with the reference spectrum of zinc oxide. The surface area of the sample, however, was only 6.5 m^2/g.

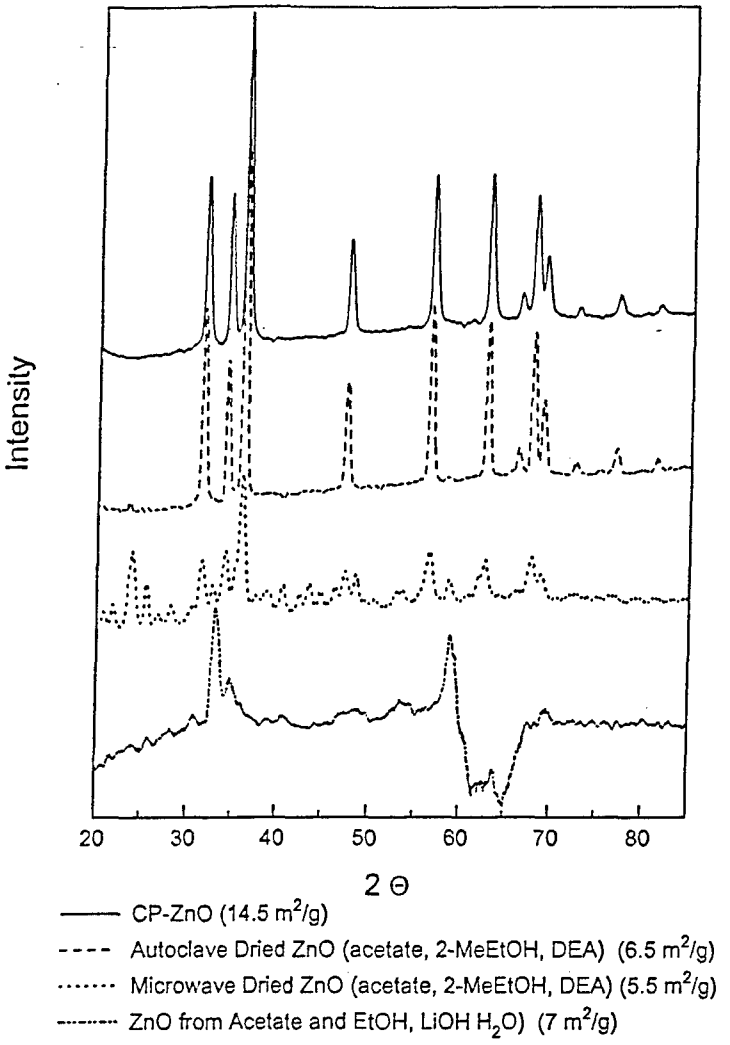

Figure 1. XRD Spectra of Zinc Oxide Prepared by Different Synthesis Methods

A thorough literature review was then conducted searching for another synthesis approach for this unique metal oxide.[27-39] The search suggested that the use of diethylzinc could provide a viable approach. The following three variations of this approach were developed, with the final resulting in a highly reactive product that surpasses any report in the literature.

(i) Diethylzinc solution (15% in Toluene) and butanol were mixed at room temperature. A vigorous reaction was observed. The solution was stirred for one hour, after which 5 ml of water in 65 ml of ethanol were added. A white precipitate was formed, that was dried in a microwave (to remove excess of the solvent) for about 20 min. The sample was studied by X-ray diffraction (XRD) and proved to be zinc oxide. The surface area of this material was 53 m^2/g.

(ii) Diethylzinc solution (15 % in toluene) and t-butanol in 30 ml of hexanes were stirred at -70°C and slowly warmed up to room temperature. During that time an evolution of gas was observed. After stirring for 2 hours at room temperature, the gas evolution stopped and the solution was left overnight without stirring. Then, 6.8 ml of water in 76 ml of ethanol were slowly added. A white precipitate was observed, that was dried in a microwave. The surface area of the resulting ZnO was 70 m^2/g.

(iii) This sample was prepared following the same procedure as (ii). The only differences were shorter reaction time and the amount of water added. Water was reduced by a factor of three. The surface area of this sample was 75 m^2/g.

The best ZnO sample, showing the highest reactivity towards the one-armed mustard, 2-chlorodiethyl sulfide (2-CEES), and paraoxon was sample (iii), the second best was (i) and the third was (ii). Refer to the following sections for supporting data. Most likely the amount of water added during the preparation plays a very important role. If too much water was added, the reactivity decreased even if the surface area was comparable. Work is continuing on developing a synthetic method to produce very high surface area ZnO. The results presented above already surpass all literature reports.

Based on these encouraging results, several additional samples of ZnO were prepared using diethyl zinc as the starting material. It is believed that the intermediate product formed is ethylzinc-t-butoxide, that upon water addition converts to ZnO. The schematic of the process is shown below.

$$Et_2Zn + t-butanol \xrightarrow{RT} [Et-Zn-t-butoxide] \xrightarrow{Water} ZnO$$

The variations in the synthesis procedure were mainly concerned with the amounts of t-butanol and water used during the reaction as well as temperature at which the reaction was carried out. It appears that the most critical process variable for the production of highly reactive ZnO powders is the amount of water used during the conversion of the intermediate product, ethylzinc-t-butoxide, to ZnO. This is probably related to the extent of hydrolysis of the ethylzinc-t-butoxide. If too little water is used, a large percentage of the alkoxy groups remain on the surface of the powder, decreasing the destructive adsorption ability. This effect was observed even for samples where the surface area was high due to smaller crystallinity of the t-butoxide/ZnO mixture. Conversely, when too much water was added, lower surface area ZnO was obtained.

In addition, there was some evidence that the molar ratio of diethyl zinc and t-butanol could play an important role. Better reactivity was obtained when a molar ratio greater than 1:1 was used. For example, a sample with a molar ratio of 1.2:1 yielded approximately a 43% improvement in the observed destructive adsorbance of paraoxon as compared with a sample with a molar ratio of 1:1. Finally, it appears that preparation temperature does not play an important role in the reactivity of the ZnO sample, because the best results were obtained with samples that were prepared at room temperature and -76°C. Further work is needed to optimize the conditions of the reaction.

Preliminary experiments were conducted to see if zinc oxide can be deposited as a thin outer layer on the AP-MgO nanocrystals, in a similar fashion as has been previously done for Fe_2O_3. Specifically, AP-MgO was added to the diethyl zinc solution containing t-butonal and pentane. Water in absolute ethanol was then added and the slurry was dried in the microwave. The resulting powder was studied by XRD and peaks associated with MgO, ZnO and possibly some $Mg(OH)_2$ were observed. The surface area of the resulting powder was 142 m^2/g which increased to 165 m^2/g upon activation under vacuum conditions.

Therefore, Nantek has developed truly novel zinc oxide materials with surface areas 3 times that of commercially available "high" surface area zinc oxide powders. In an attempt to even further expand the reactive capacity, custom design and synthesis of [ZnO]AP-MgO materials yielded a 7-fold increase in surface area and complete destruction of paraoxon within two minutes while commercial ZnO exhibited only modest reactivity after 20 hours of exposure (the following section provides additional detail).

2.2 Ambient Condition Destructive Adsorbent Test Results

During the Phase I Research, extensive testing of the destructive adsorbent performance of a broad array of nanoparticle samples was conducted. These tests were conducted using mimics of nerve agents such as paraoxon and 2-CEES, the one-armed mustard. Figure 2 provides an illustration of the chemical composition of the military agents and their corresponding mimics.

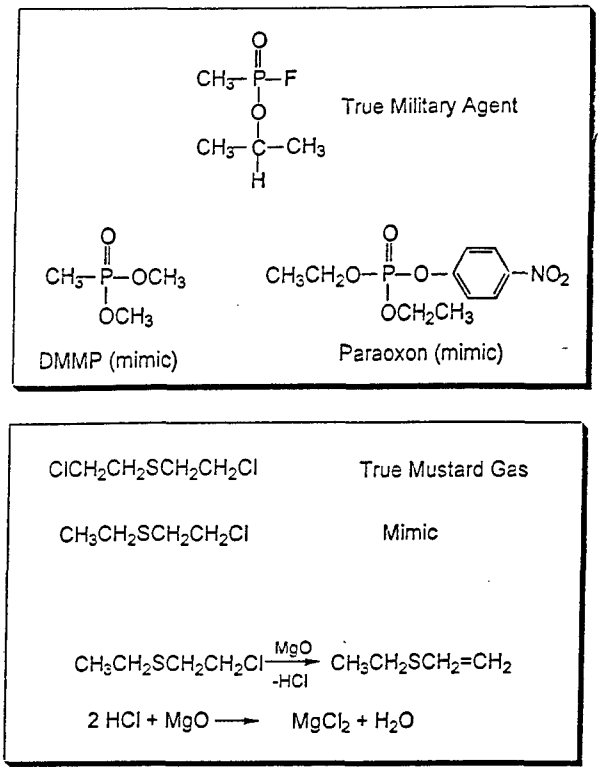

Figure 2. Military Agents and Their Mimic Counterparts

2.2.1 Analysis of the Paraoxon-Adsorbent Reaction Using UV-Vis

In UV-Vis/paraoxon experiments, 0.1 g of the oxide (unless otherwise specified) was placed in a round bottom flask and purged with nitrogen. To the powder, 100 ml of freshly distilled pentane was added and the solution was again purged with nitrogen to remove moisture and air from the environment. Then, 4.5 μL of paraoxon was added and the solution was stirred with a magnetic stirrer. The disappearance of the paraoxon was investigated over time, by analyzing the UV-Vis spectra in the 200-400 nm region. Paraoxon gives a distinctive peak at 267 nm, and a product of decomposition, p-nitrophenol can usually be seen at 225 nm. This product, however, briefly appears and is presumed to be quickly back-adsorbed on the oxide surface. A blank test (without oxide added to the flask) was carried out under the same conditions.

Preliminary Test Trials

In the initial trials, a broad array of readily available samples (either commercial samples or particles previously produced at Nantek's laboratory) were tested for paraoxon decomposition as detailed in Table I. Figure 3 shows the disappearance of paraoxon on these sample compounds over time. In these experiments, the reaction was monitored over a period of 24 hours. After the best samples were chosen, more detailed studies of the initial reaction of the adsorbent/mimic were carried out. In addition to the UV-Vis spectra analysis, adsorption of the paraoxon was readily visible on most of the white powder samples due to the change in color of the powder from white to bright yellow. Note that paraoxon is a pale yellow, oily substance and its color does not duplicate the bright yellow observed. However, the anion $O_2NC_6H_4O^-$ is bright yellow, and this observation coupled with IR data strongly suggest that this anion is formed very quickly on the surface of some of the nanoscale oxide adsorbents.

Some general conclusions can be drawn from Figure 3. Materials with higher surface area appear to adsorb much better than those with lower surface area; however, some discrepancies were observed. For example, the commercial zinc oxide (CM-ZnO) particles have a slightly higher surface area than Nantek's

Table I. Samples Studied in Preliminary Mimic Adsorption

SAMPLE DESCRIPTION	DESIGNATOR	SURFACE AREA (m^2/g)
Autoclave Prepared Magnesium Hydroxide	AP-$Mg(OH)_2$	800
Autoclave Prepared Calcium Hydroxide	AP-$Ca(OH)_2$	90
Commercial Copper Oxide	CM-CuO	<1
Commercial Nickel Oxide	CM-NiO	4
Commercial Iron Oxide	CM-Fe_2O_3	8
Commercial Zinc Oxide	CM-ZnO	24
Conventionally Prepared Zinc Oxide	CP-ZnO	20
Commercial Titanium Dioxide	CM-TiO_2	42

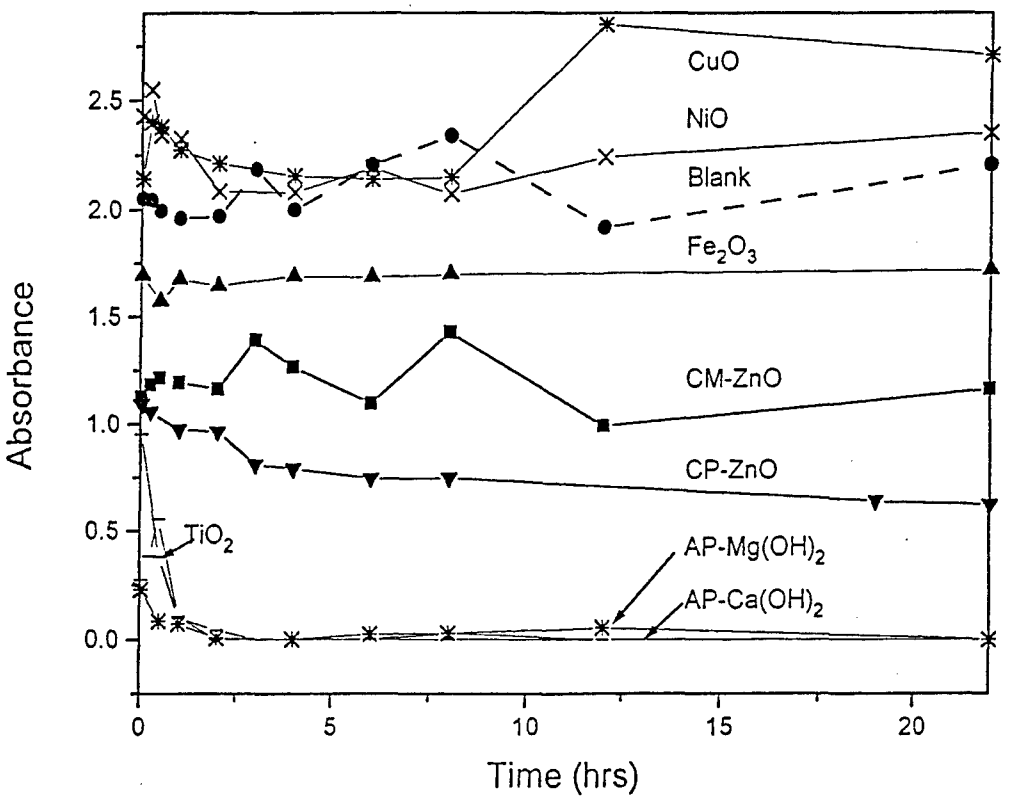

Figure 3. Disappearance of Paraoxon (4.5μL) on Different Metal Oxides (0.1g)

conventionally prepared (CP-ZnO) samples. However, adsorption of paraoxon is actually poorer on the higher surface area, commercial samples (CM-ZnO). Particles of CM-ZnO are believed to be more spherical in microstructure, with fewer defect sites. This may be the reason for the lower reactivity as compared to Nantek's conventionally prepared samples. It is anticipated that autoclave prepared samples of ZnO would be even more reactive than the CP-ZnO samples due to their substantially increased number of surface defect and edge sites.

Titanium dioxide (TiO_2) samples were also studied, and adsorbed paraoxon reasonably well. (However, later tests with 2-CEES, the mustard mimic, were not successful, and so TiO_2 is not considered a good candidate for the final formulation). Finally, moderate surface area copper and nickel oxides did not adsorb any paraoxon on the surface. Iron oxide demonstrated some adsorption capability, however to a lesser extent as compared with magnesium, calcium, zinc and titanium oxide samples.

In addition, comparative studies between hydroxide and oxide samples of magnesium and calcium were studied. On a gram/gram basis, the metal oxides were more reactive than their hydroxide counterparts. This is believed to be due to the presence of stronger Lewis Base sites on the oxide samples (as a result of the presence of coordinately unsaturated oxide and metal ions on edge and defect sites).

Extensive Test Trials

Based on the encouraging results presented above, extensive testing of the paraoxon-adsorbent reaction was conducted on a number of nanoparticle samples. The primary objective was to further characterize the performance of the adsorbents that demonstrated efficacy in the preliminary testing (i.e., CaO, MgO, ZnO, and TiO_2) as well as to study the room temperature behavior of nanoparticle composite materials. In Nantek's previous work, composite metal oxide nanoparticles coated with a monolayer of a different metal oxide (typically a transition metal) provided enhanced destructive adsorbent behavior at high reaction temperatures. The composite behavior at lower temperatures had not been previously characterized and could be of considerable interest for this protective application.

Table II presents the samples studied during this stage of the research. In most cases, 0.1 g of metal oxide powder was used for the experiment, unless otherwise specified. The results of the paraoxon studies are found in Figures 4-8. Figure 4 shows the results of paraoxon exposure to various magnesium oxide samples including autoclave-prepared, conventionally-prepared and iron coated composite materials. The AP-MgO nanoparticles appear to outperform all other magnesium samples tested. The paraoxon was completely adsorbed on the AP-MgO sample before the first reading could be measured at 2 minutes after exposure. The exceptional performance has been repeated in several test trials and is probably due to material's very high surface area of 562 m^2/g. The iron oxide coated MgO sample (Fe/AP-MgO with a surface area 360 m^2/g) also behaved very well. After 20 minutes, no paraoxon was observed in the reaction flask. The amount of iron oxide was about 1% by weight of the sample. The conventionally prepared MgO samples (340 m^2/g) also adsorbed paraoxon very efficiently.

The data obtained for calcium oxide is shown in Figure 5. The iron oxide coating enhances the performance for both conventional and autoclave-prepared calcium oxide. For the iron coated AP-CaO sample, only about 10% of the paraoxon was present after 2 hours reaction (based on the height of the paraoxon peak). CP-CaO did not behave as well, even though its surface area was comparable to AP-CaO (about 120 m^2/g). However, when iron oxide was present, the surface area of CP-CaO decreased (from 110 m^2/g to 68 m^2/g) but the amount of adsorbed paraoxon was much higher. The iron coating either enhances the intrinsic surface reactivity, and/or it protects the core CaO particles from adventitious water, thus enhancing destructive adsorbent activity over the uncoated samples. This effect is likely to be important for the skin-protection system under development, and further work is needed in order to understand this interesting effect.

Table II. Samples Studied for Paraoxon Decomposition

SAMPLE DESCRIPTION	DESIGNATOR	SURFACE AREA (m^2/g)
Autoclave Prepared Magnesium Oxide	AP-MgO	562
Conventionally Prepared Magnesium Oxide	CP-MgO	340
Iron coated, Autoclave Prepared Magnesium Oxide	Fe/AP-MgO	360
Autoclave Prepared Calcium Oxide	AP-CaO	112
Iron coated, Autoclave Prepared Calcium Oxide	Fe/AP-CaO	100
Conventionally Prepared Calcium Oxide	CP-CaO	110
Iron coated, Conventionally Prepared Calcium Oxide	Fe/CP-CaO	68
Zinc Oxide - (i)	ZnO (I)	53
Zinc Oxide - (ii)	ZnO (ii)	70
Zinc Oxide - (iii)	ZnO (iii)	75
Commercial Zinc Oxide	CM-ZnO	24
Conventionally Prepared Zinc Oxide	CP-ZnO	20
Titanium Oxide - Activated at 200C	TiO_2 (act.)	42
Titanium Oxide - Not Activated	TiO_2 (N.A.)	44
Autoclave Prepared Titanium Oxide	AP-TiO_2	127

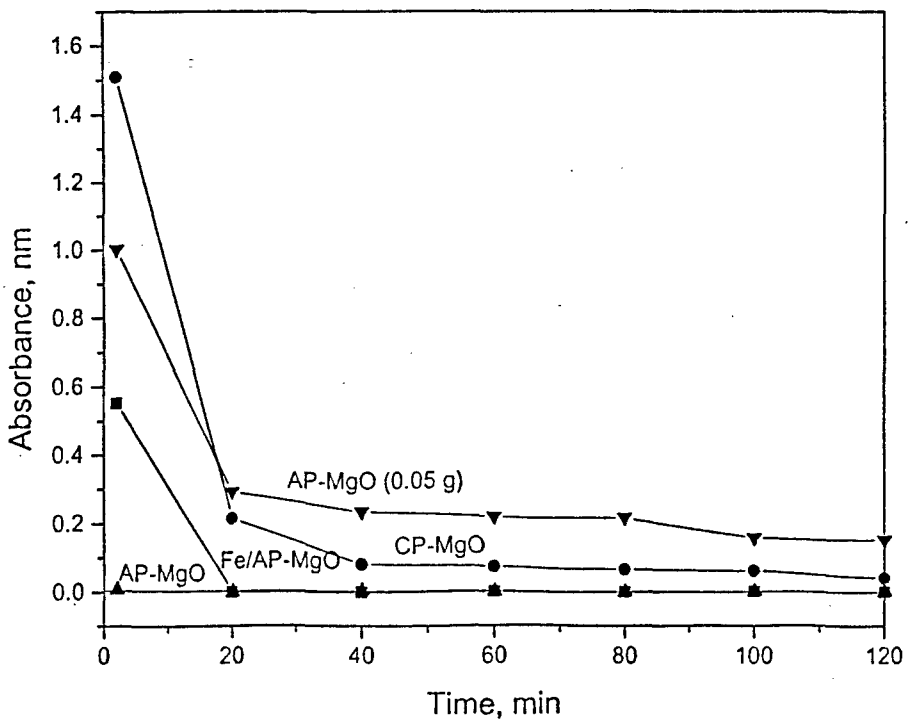

Figure 4. Disappearance of Paraoxon (4.5 μL) on Magnesium Oxide Samples

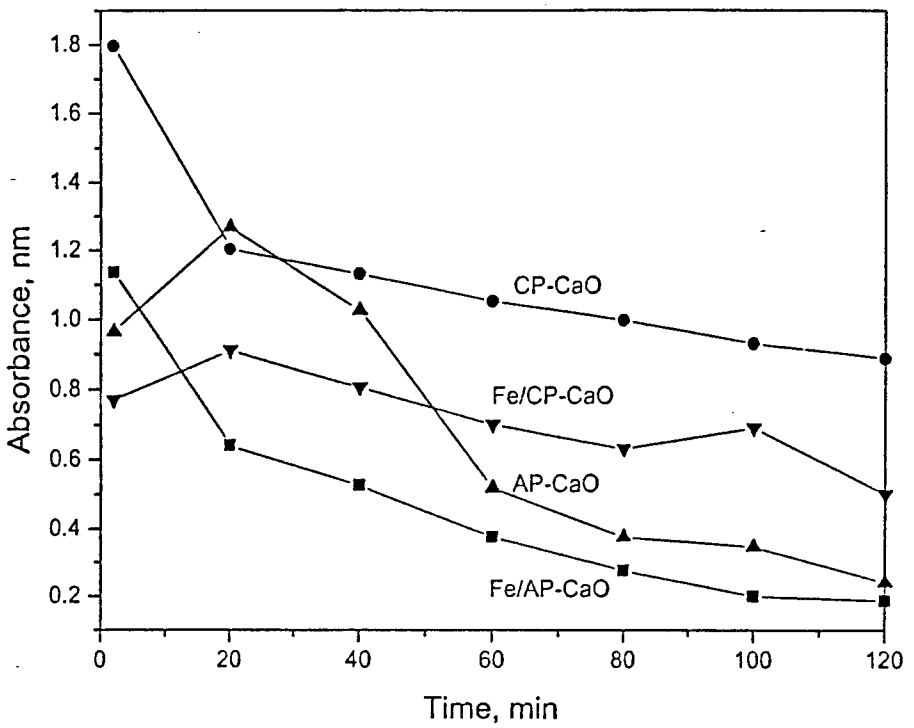

Figure 5. Disappearance of Paraoxon (4.5 μL) on Calcium Oxide Samples (0.1g)

In our previous work on higher temperature experiments, coating AP-MgO or AP-CaO with Fe_2O_3 caused an increase in destructive adsorbent capacity of chlorocarbons, acid gases, and organophosphorus compounds. We attribute this behavior to catalysis of thermodynamically favored solid-state ion-ion exchange.[40,41] Also, by coating high surface area AP-samples with a different metal oxide such as Fe_2O_3, much higher surface area material can be obtained than is possible with iron alone. More recently, this enhancement effect has been seen during our room temperature reaction studies. Therefore in the Phase II Research, further investigation of a series of combinations, such as AP-MgO coated with ZnO and Fe_2O_3, is warranted. It is anticipated that destructive adsorbent capacities may be significantly enhanced due to the very high surface areas and perhaps a protecting effect so that the MgO or CaO core particles are less susceptible to hydrolysis by water entering the reaction zone (the protective cream).

Several samples of zinc oxide were tested for adsorption of paraoxon (see Figure 6). The decomposition ability of ZnO is not solely dependent on its surface area, but also on the method of preparation, particularly the amount of water that is added during the synthesis. The conventionally prepared (CP-) and commercial (CM-) zinc oxide powders demonstrated very similar decomposition capability. The ZnO prepared using smaller quantities of water, referred to as method (iii) in the previous section, was about three times more efficient.

Figure 7 shows results obtained for titanium dioxide (Degussa). If an excess of TiO_2 is present (0.4 grams instead of 0.1 g), then paraoxon can be completely destroyed during the first few minutes of exposure. Due to these encouraging results, autoclave prepared samples were produced for further testing. Essentially, a solution of distilled water, concentrated nitric acid, and methanol were added to methanol and neat titanium (IV) butoxide. The formed gel was aged overnight and then hypercritically dried in the autoclave. The powder obtained was heat treated under a flow of nitrogen and oxygen to fully convert the powder to TiO_2. The resulting powder had a surface area of 127 m^2g. The paraoxon decomposition results

for these high surface area TiO_2 samples were quite promising at the time. While the sample was not as reactive as Nantek's AP-MgO material, it performed significantly better than the best ZnO sample and the iron coated AP-CaO sample.

Figure 8 provides data for the best oxides from each of the groups tested for the decomposition of paraoxon, as well as the blank test. In addition, Table III provides a tabular summary of the paraoxon decomposition at 2 hours and 20 hours after exposure. Magnesium and calcium oxides, both coated and uncoated, were very active with essentially total disappearance of paraoxon within the 20 hour exposure period. In fact, for a majority of the samples decomposition occurred very rapidly with near complete disappearance within the first two hours of testing. Most notably, complete disappearance of the paraoxon was observed before the initial reading at two minutes for Nantek's AP-MgO material. High surface area ZnO, TiO_2, and zinc coated AP-MgO performed quite well for paraoxon decomposition. Non-activated [ZnO]AP-MgO nanocrystals, having a surface area of 142 m^2/g, destroyed the paraoxon within forty minutes of exposure, while the activated material (165 m^2/g) destroyed all of the mimic compound within the first two minutes following exposure.

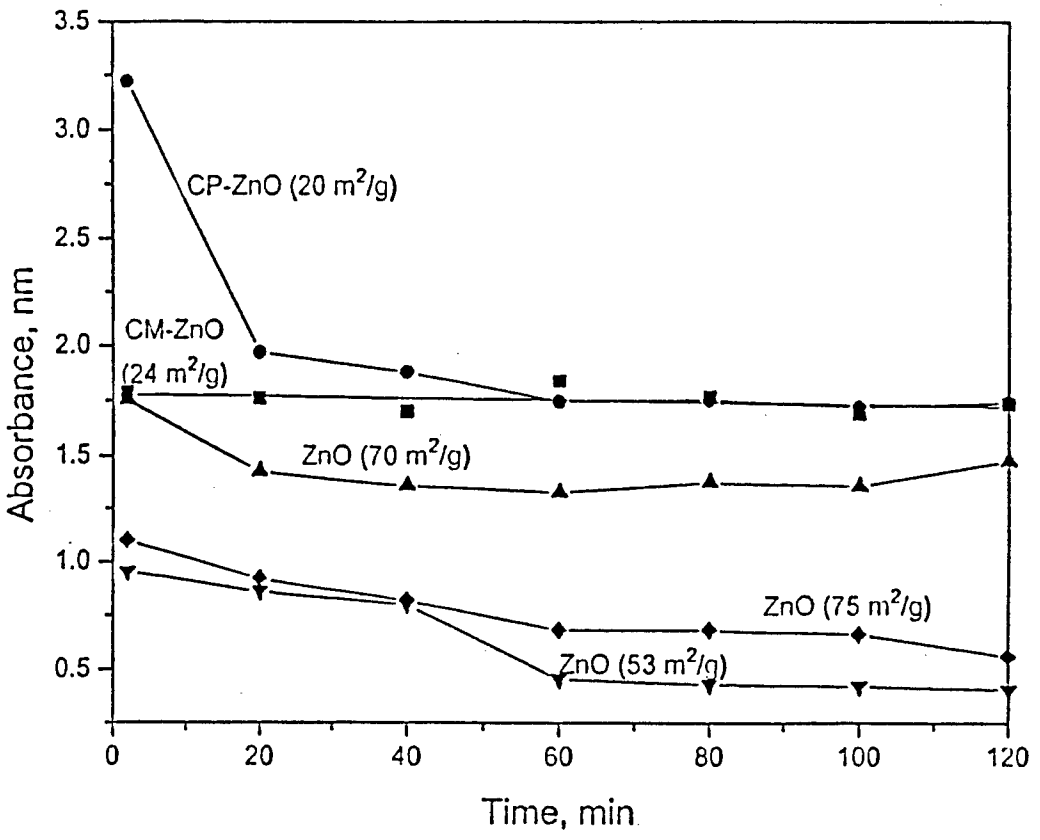

Figure 6. Disappearance of Paraoxon (4.5μL) on Zinc Oxide Samples (0.1g)

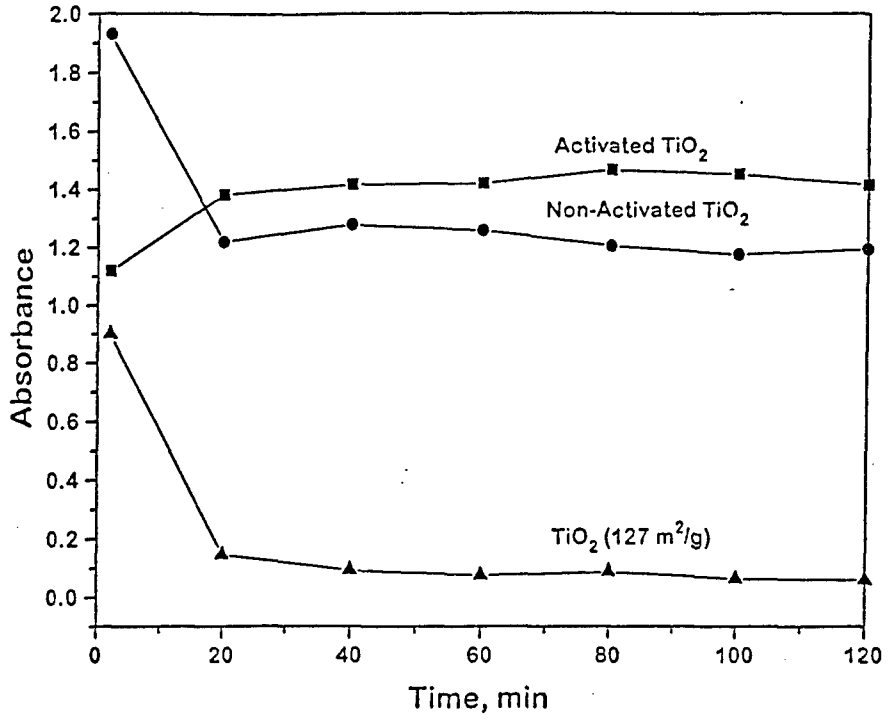

Figure 7. Disappearance of Paraoxon (4.5μL) on Titanium Oxide Samples (0.1g)

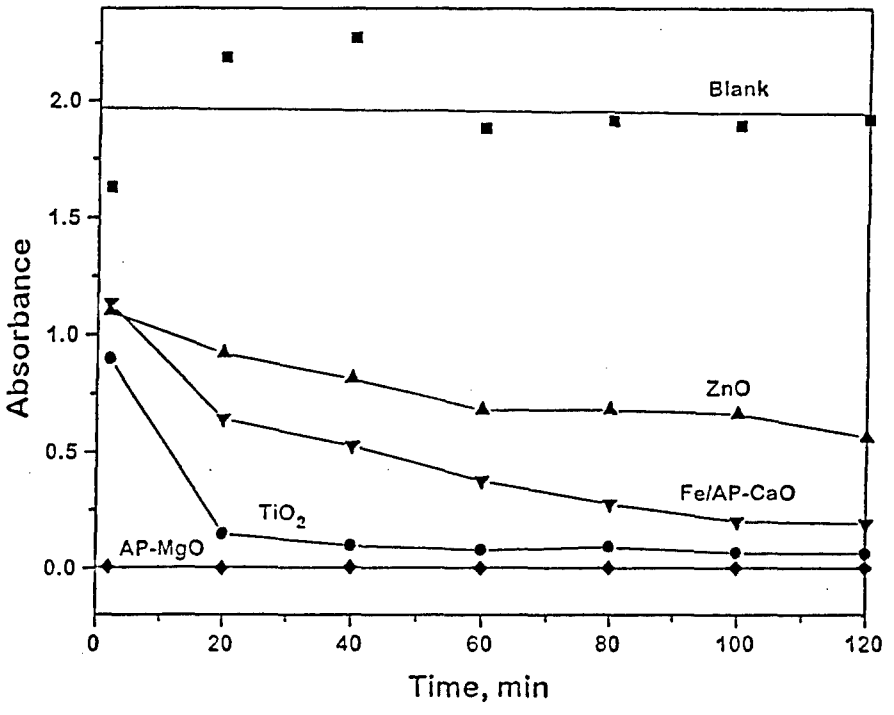

Figure 8. Disappearance of Paraoxon (4.5 μL) on Various Metal Oxide Samples (0.1g)

Table III. Decomposition of Paraoxon on Various Metal Oxides, After 2 and 20 Hours

Sample	Surface area (m^2/g)	Peak Intensity After 2 Hours	Peak Intensity After 20 hours
Blank	-	1.918	1.935
AP-MgO	562	0	0
CP-MgO	340	0.071	0
Fe/AP-MgO	360	0	0
Zn/AP-MgO	142	0	0
Zn/AP-MgO activated	165	0	0
AP-CaO	112	0.240	0
Fe/AP-CaO	100	0.187	0
CP-CaO	110	0.887	0.044
Fe/CP-CaO	68	0.487	0
ZnO (I)	53	0.406	0.229
ZnO (ii)	70	1.729	1.628
ZnO (iii)	75	0.496	0
CM-ZnO	24	1.739	2.432
CP-ZnO	20	1.473	0.918
TiO_2 (activated)	42	1.412	1.297
TiO_2 (not activated)	44	1.172	1.309
AP-TiO_2	127	0	0

Sample Analysis After Exposure to Paraoxon

After the reaction with paraoxon, a number of inspections were conducted to find additional evidence that the oxides are decomposing and not just adsorbing the toxins on the surface of the powders. As discussed earlier, adsorption of the paraoxon was readily visible on most of the white powder samples due to the change in color of the powder from white to bright yellow. This was believed to be due to formation of the anion, $O_2NC_6H_4O^-$, which is also bright yellow. The color change was most dramatic for the magnesium samples and weakest for the low surface area titanium samples, correlating to the data presented above, and thus provides a clear indication that the paraoxon is being destroyed.

Solid products were further studied by XRD and IR spectroscopies. The XRD patterns did not exhibit any changes in the metal oxide structure. This was anticipated because at room temperature we would not expect much solid state diffusion and ion-ion movement. In other words, only the surface of the oxide reacts. However, IR spectra of the solid product (IR detects the surface adsorbed species) did show some changes before and after reaction. Figure 9 shows the difference spectrum between paraoxon reacted AP-MgO versus unreacted AP-MgO. A comparison of this difference spectrum can readily be made with the pure paraoxon spectrum provided. Peak assignments for IR spectrum of paraoxon are given in Figure 10. Some adsorptions for paraoxon have disappeared upon reaction, and a strong ν_{O-H} band (3500 cm^{-1}) is present, showing the generation of new species on the surface. It is clear that the nerve agent mimic, paraoxon, has reacted and it is the "fragments" that are on the surface. Further work is needed in order to elucidate what these fragments are.

2.2.2 Adsorption of Mimics Using Activated Carbon

During the Phase I effort, Nantek performed preliminary benchmarking studies with a known adsorbent, activated carbon having an approximate surface area of 900 m^2/g. The same test conditions were utilized during the carbon testing, namely 0.1 g of the powder was dissolved in 100 ml of pentane to which 4.5 µL of paraoxon was added. The activated carbon adsorbed the paraoxon well, as anticipated. After about one hour, all of the paraoxon was adsorbed. However, when 10 µL of paraoxon was added to

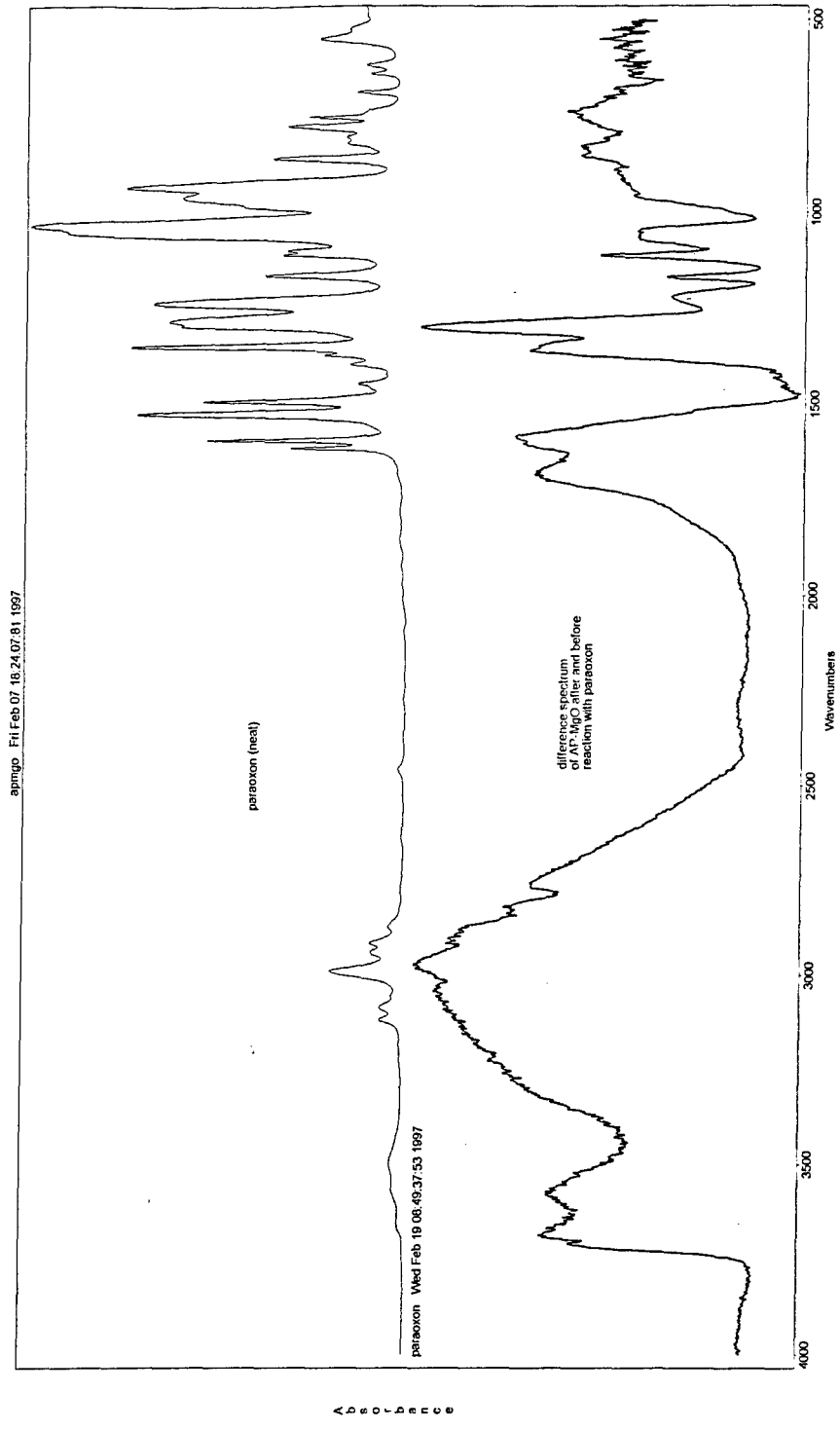

Figure 9. Comparison of AP-MgO Difference Spectrum Before and After Reaction with Paraoxon

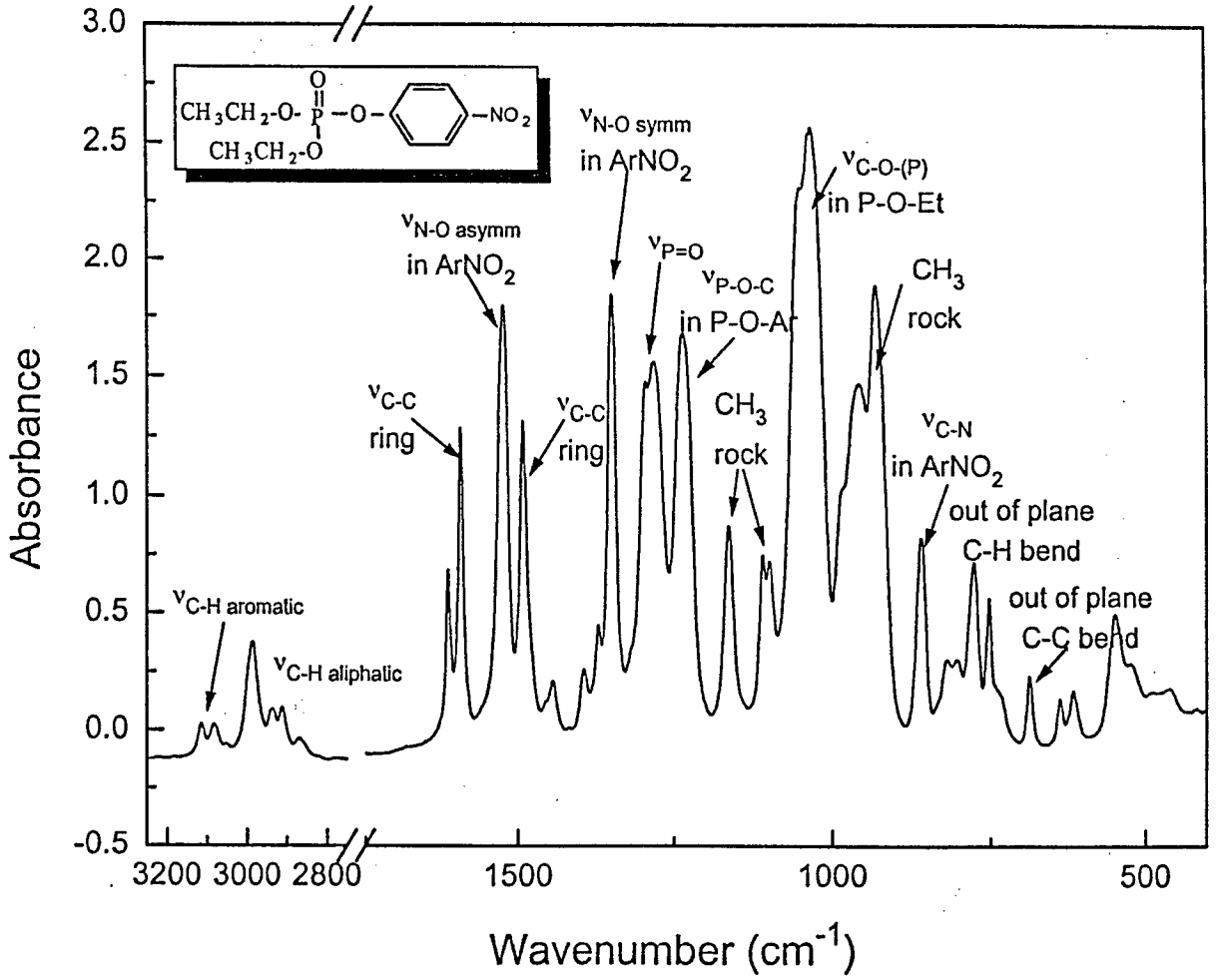

Figure 10. IR Spectrum of Neat Paraoxon with Peak Assignments

0.1 g of the powder, only partial adsorption was observed. The same experiment was carried out with 15, 30, and 50 μL of paraoxon (per 0.1 g of activated carbon). However, in all three cases the absorbance of paraoxon was too high due to its high residual concentration, and thus out of range of the UV-vis spectrophotometer.

For comparison purposes, similar experiments were conducted with Nantek's AP-MgO material that has a surface area of approximately 400 m^2/g. It was found that AP-MgO works much better than activated carbon despite its lower surface area. AP-MgO was able to completely adsorb/decompose 15 μL of paraoxon after 1 hour of exposure, whereas little adsorption was observed using the activated carbon. Interestingly, when AP-MgO was used with larger amounts of paraoxon, the peak of p-nitrophenol, a by-product of paraoxon decomposition, became more prominent. Most likely during the decomposition, p-nitrophenol is formed and subsequently back-adsorbed onto the surface if enough of the surface sites are still available. When larger amounts of paraoxon were used, the formed product could not completely adsorb on the surface and was therefore released into the pentane solution. Table IV and Figure 11 provide additional comparative data.

Table IV. Comparison of the Adsorption of Different Amounts of Paraoxon on AP-MgO (S.A. of 400 m^2/g) and activated carbon (S.A. of 900 m^2/g)

Sample	μL of paraoxon	Intensity of the paraoxon peak after 2 hours	Intensity of the paraoxon peak after 20 hours
AP-MgO	4.5	0	0
AP-MgO	10	0	0
AP-MgO	15	0.027	0
AP-MgO	30	out of range (max=5)	3.543
Activated Carbon	4.5	0	0
Activated Carbon	10	1.520	1.205
Activated Carbon	15	out of range (max=5)	2.729

After the paraoxon reaction was complete, the powders were filtered in a glove bag to minimize exposure to moisture in the atmosphere and a pellet for IR studies was made. As discussed in the previous report, the IR spectrum of AP-MgO changes completely upon adsorption of paraoxon, and resembles the spectrum of p-nitrophenol adsorbed on MgO. The only difference observed was a broad band at 1231 cm^{-1}, potentially due to P-O-C or P=O stretching. Extensive analysis of the surface geometry and chemical changes will need to be conducted during the Phase II Research to confirm these preliminary findings.

When the paraoxon was adsorbed on activated carbon, a very different spectrum was observed as shown in Figure 12. Preliminary extraction techniques were used to characterize the surface residues on the carbon sample. Methanol, a highly polar solvent, was added to the solid product in an attempt to remove the paraoxon residue. The extract was filtered and injected into a GC-MS for analysis. For comparison, the spectra of the starting compound, paraoxon, and the product of reaction, p-nitrophenol were also injected into a methanol solution. However, the methanol extraction approach was unsuccessful at removing the paraoxon species from the surface of the carbon product.

To further elucidate the species that are on the surface after reaction, other extraction procedures were attempted. Toluene was added to the solid reaction product (AP-MgO and activated carbon after reaction with 10 μL of paraoxon) and the samples were sonicated for 20 minutes to remove all species from the surface. The extract was then filtered using a syringe filter and injected into the GC-MS. For AP-MgO, no additional peaks were observed; however, in the case of the activated carbon, some non-decomposed paraoxon was detected.

In summary, Nantek's AP-MgO reactant appears to be significantly more adsorbent than activated carbon. This finding was not necessarily expected, since the carbon material with its high surface area and large pore density is recognized for its adsorbent capability. On a preliminary basis, we attempted to confirm our belief that activated carbon adsorbs yet does not react or destroy the paraoxon. We have demonstrated that special high surface area, metal oxide materials do indeed destroy the highly toxic substances through the formation of the reaction by-products, p-nitrophenol for paraoxon decomposition and vinyl sulfide for the one-armed mustard decomposition. The preliminary results do indicate that the solid products are indeed quite different. New extraction techniques for elucidation of the species on the surface of the activated carbon will need to be investigated in the Phase II effort.

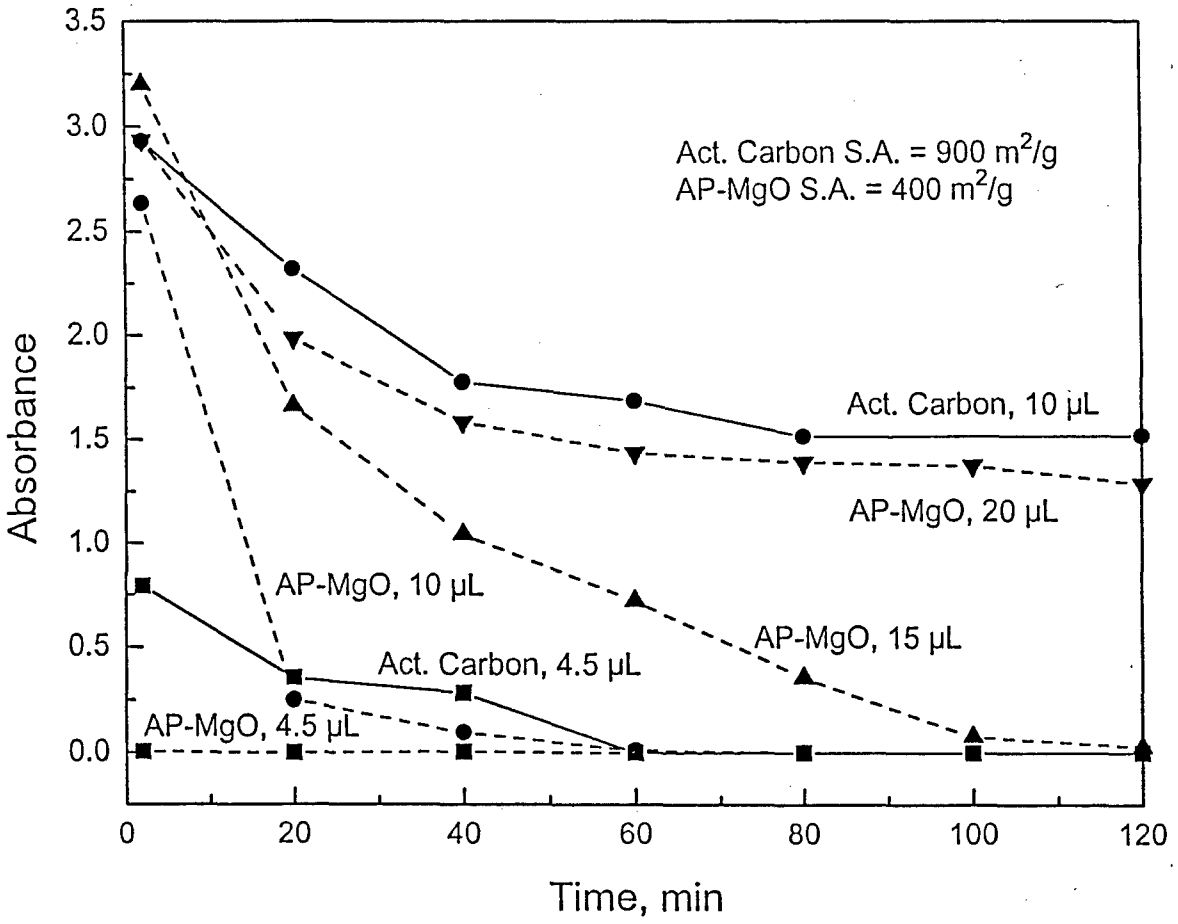

Figure 11. Adsorption/Decomposition of Different Amounts of Paraoxon on Activated Carbon and Nantek's AP-MgO Reactants

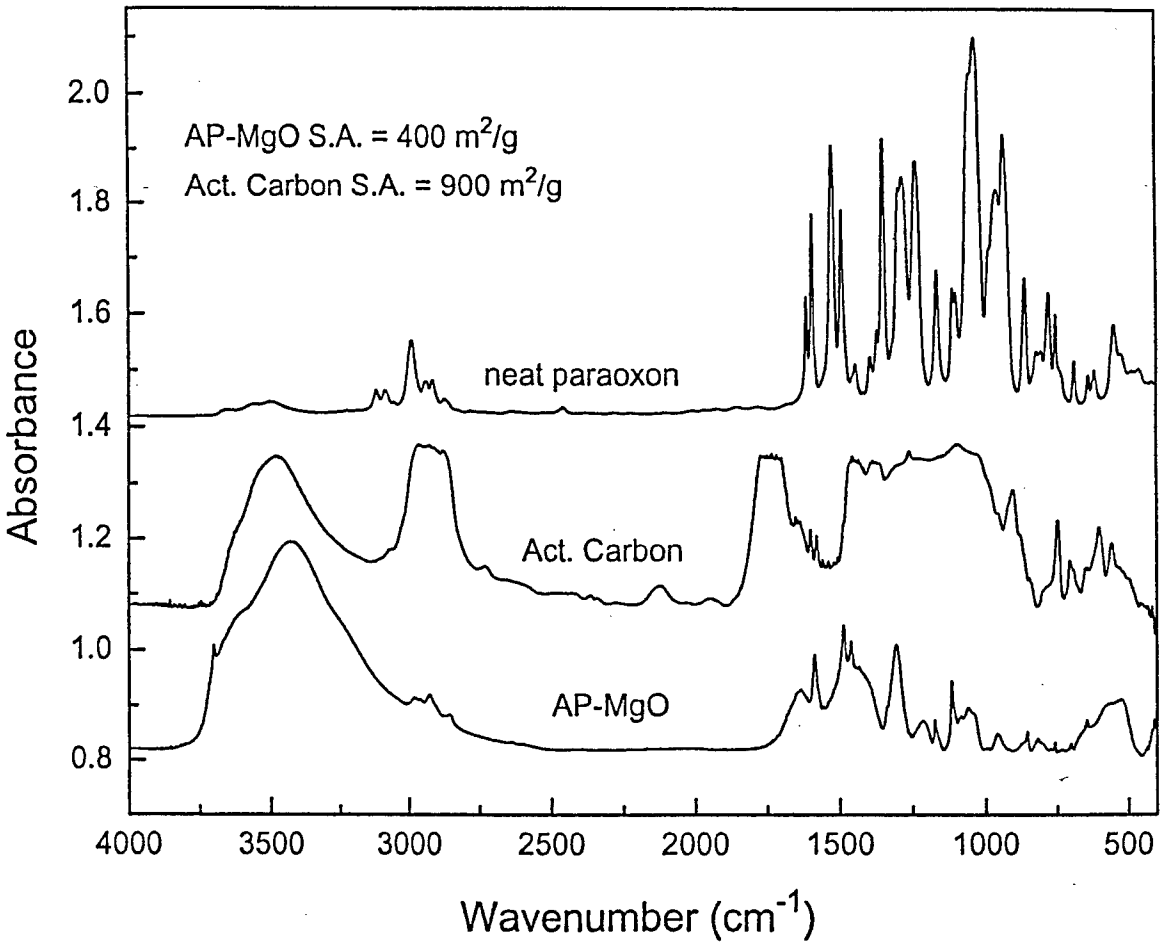

Figure 12. IR Spectra of the Solid Products After Reaction of Paraoxon (10 L) on Activated Carbon and Nantek's AP-MgO Reactants (A spectrum of neat paraoxon is shown as a reference)

2.2.3 Decomposition of 2-Chlorodiethyl Sulfide (2-CEES) on Various Metal Oxides

Extensive Test Trials

In these experiments the samples exhibiting the best adsorbent activity in the paraoxon studies were used to study the dechlorination of 2-chlorodiethyl sulfide (2-CEES), a mimic of mustard gas. This process can be monitored using IR-spectroscopy by observing a growth of a peak assigned to ethylvinyl sulfide, a decomposition product. It is necessary to observe the product of the reaction since the disappearance of 2-CEES cannot be monitored directly, since the majority of the peaks of 2-CEES superimpose the peaks of ethylvinyl sulfide. The only significant difference between 2-CEES spectrum and ethylvinyl sulfide spectrum is the peak at 1595 cm^{-1} attributed to the double bond of ethylvinyl sulfide. The observation of the growth of this peak was therefore used as a fingerprint in the decomposition of 2-CEES.

The 2-CEES decomposition experiment was conducted in the following manner. A gas IR cell was attached to a round bottom flask, and 0.1 g of the metal oxide was placed in the flask that was subsequently evacuated (to a few millitorr pressure). Then, 14 μL of 2-CEES was introduced (injected through a septum placed on the neck of the flask) and the cell was placed in the IR spectrophotometer. The scans were taken after 5, 15, 30 minutes and then every 30 minutes up to 5 hours. The last measurement was taken after 20

hour exposure of metal oxide to 2-CEES. The blank test (without metal oxide present in the cell) showed that 2-CEES does not decompose by itself under these experimental conditions.

The test results are presented in Table V and Figure 13 for the calcium, magnesium, and zinc oxides reactants. Figure 13 shows the comparison between different types of metal oxides used and Table V gives the intensity of the vinylethyl sulfide peak after 5 and 20 hours of exposure. It should be noted that the 2-CEES decomposition test measures a decomposition product. Thus, increased intensity versus time suggests higher decomposition activity.

It is particularly interesting that the CaO samples are very reactive, especially the iron oxide coated sample, Fe/AP-CaO. Also note that ZnO(iii) produced with a minimal amount of water is superior to ZnO(i). We are currently developing continuously improved methods of preparation of higher surface area ZnO, and believe that these results encourage further work be done on specialized ZnO synthesis. Titanium oxide, either commercial or autoclave prepared did not show any activity towards 2-CEES despite the fact that it was very reactive when exposed to paraoxon. As such, further development of titanium oxide reactive nanoparticles is likely not warrented.

A rather peculiar result is that the best sample for paraoxon destructive adsorption (AP-MgO) behaved unexpectedly in the 2-CEES reaction. In a very short time, ethyl vinyl sulfide appeared in the spectrum, but it did not increase over time as with the other samples tested. Recall that the surface area of AP-MgO is very high (> 500 m^2/g). We suspect that this curious result is due to the establishment of a rapid equilibrium where 2-CEES is destroyed, but the ethylvinyl sulfide is also largely adsorbed on the AP-MgO surface. This tentative conclusion, of course, needs further confirmation. Indeed recent results indicate that under these experimental conditions, 85% of the total 2-CEES was destroyed. Complete destruction may be inhibited by the back-adsorption of the ethylvinyl sulfide. Phase II Research will be directed at this problem; new nanoparticle formulations that are more reactive with 2-CEES, but less able to back-adsorb the vinyl compound will be targeted. Based on the data at present, CaO and ZnO or combinations of these two may be important to investigate.

Similar behavior was observed for the CP-MgO sample but to a lesser extent. In other words, back-adsorption of ethylvinyl sulfide occurred at a lower rate than that observed during the AP-MgO experiments. This is possibly attributed to the lower surface area of the CP-MgO material. However, the differences in surface morphology between CP- and AP- materials are believed to be more important. Recall that AP-MgO particles can be characterized as highly irregular materials with many edge and surface defect sites. CP-MgO particles, on the other hand, are more crystalline in nature with planar surfaces containing substantially fewer edge and surface defects. It is believed that the highly irregular, non-crystalline morphology is primarily responsible for the superior surface reactivity.

Table V. Formation (intensity) of the ethylvinyl sulfide peak during 2-CEES decomposition on various metal oxides.

Sample	Surface area(m^2/g)	Absorbance after 5 hrs	Absorbance after 20 hrs
Fe/AP-CaO	100	58.3	186.1
CP-CaO	110	52.2	130.5
AP-CaO	92	39.1	113.3
ZnO(i)	53	14.7	34.7
ZnO(iii)	75	30.0	73.9
AP-MgO	562	20.6	52.5
CP-MgO	340	19.9	41.1
AP-TiO_2	127	0	0

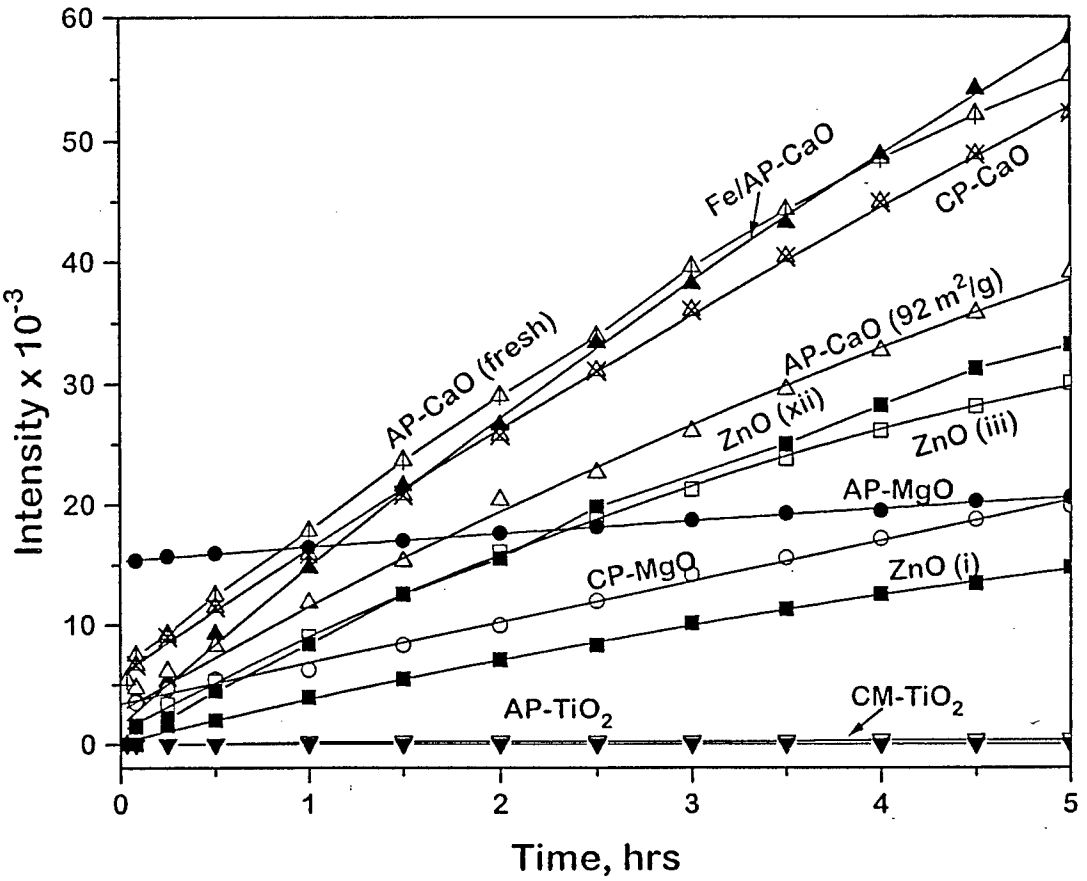

Figure 13. Appearance of Ethylvinyl Sulfide During 2-CEES Decomposition on Various Metal Oxides

Sample Analysis After Exposure To 2-CEES

The solid products of reaction were studied by XRD and IR-spectra for evidence of decomposition. As with paraoxon decomposition, no metal oxide structural changes were observed by XRD due to a small ratio of 2-CEES to metal oxide. On the other hand, the infrared spectroscopy showed some differences between the oxides before and after the exposure to 2-CEES. Figure 14 shows the IR spectra of CaO and iron oxide coated CaO before and after reaction. Two differences can be easily seen. First, we can observe the formation of associated hydroxyl groups, as seen by the growth of a broad band at 3300 cm^{-1} and secondly, the broadening of a peak at 1082 cm^{-1} (assigned to calcium carbonate on the surface of CaO). To emphasize these differences we removed the IR spectrum of the oxide before reaction from the spectrum of the same oxide after reaction (Figure 15). Although the differences appear more pronounced, they do not correspond to a simple adsorption of 2-CEES or ethylvinyl sulfide on the surface (shown in the top spectrum). Therefore, it is clear that the mustard mimic, 2-CEES, is not simply adsorbed. It is destroyed on the surface of the nanoscale oxide particles.

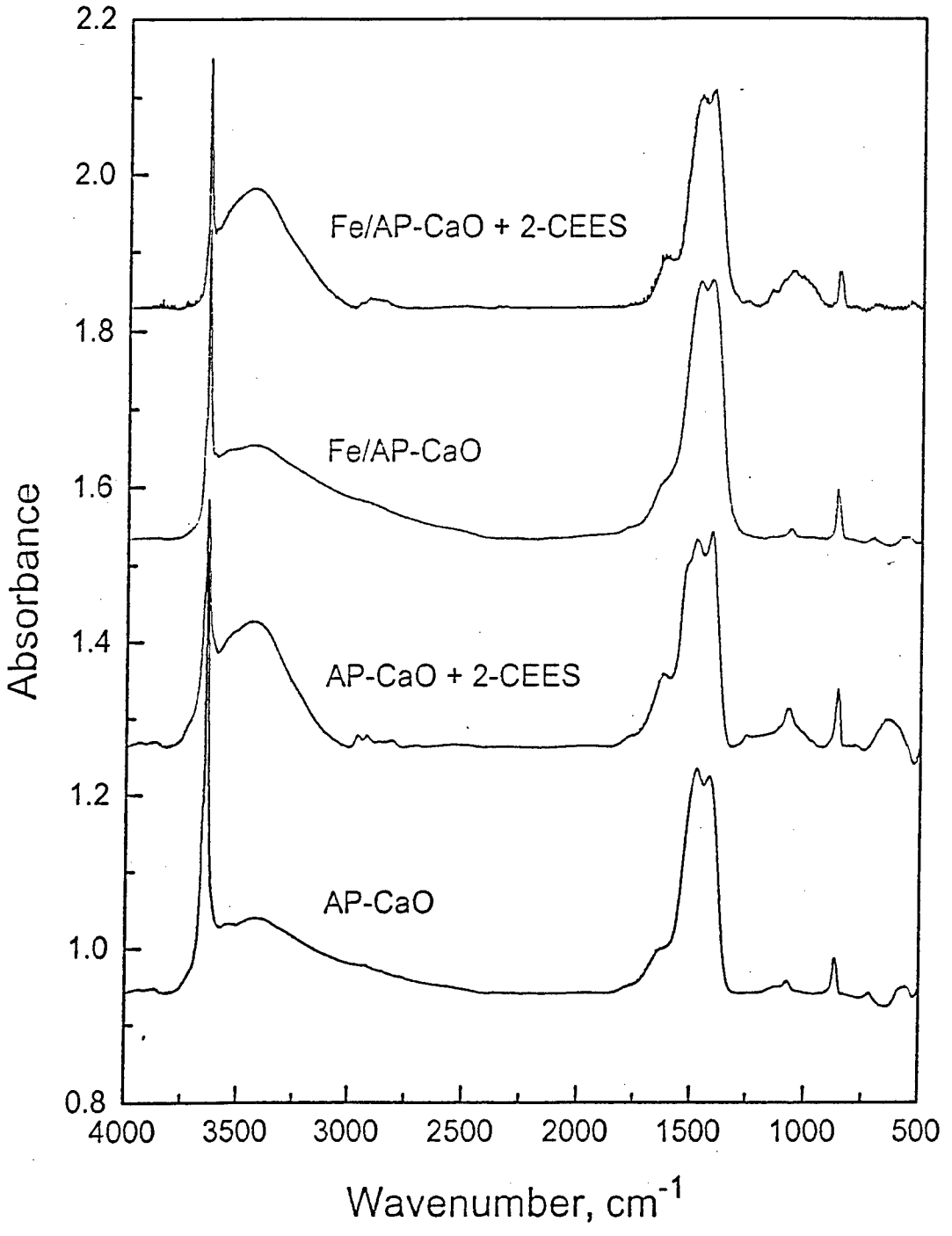

Figure 14. IR Spectra of the Solid Before and After Reaction with 2-CEES, the Mustard Mimic

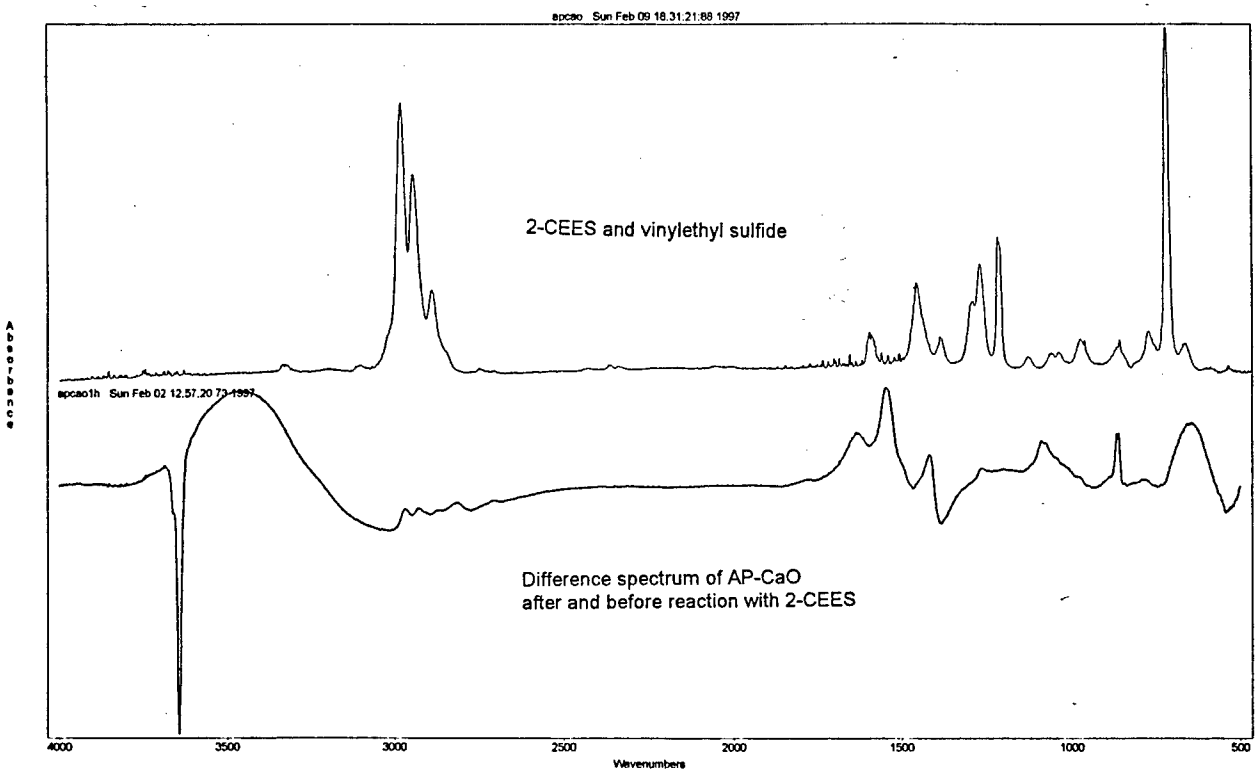

Figure 15. Comparison of the AP-CaO Difference Spectrum Before and After Reaction with 2-CEES, the Mustard Mimic

2.3 Physical Compatibility of the Metal Oxides in the Base Cream

Magnesium, calcium and zinc oxides were mixed with the base cream provided by the Army and an XRD of the paste was taken. For comparison, a diffraction pattern of the pure cream was also recorded. The cream by itself gives a high baseline in the spectrum. However, if enough oxide is present in the cream, it is possible to distinguish between the oxide pattern and the base cream. It appears that the cream does not change upon mixing with the oxide but the spectrum of MgO somewhat coincides with the cream spectrum. On the other hand, calcium oxide and zinc oxide give clearly distinctive peaks at different angles than the cream, as is shown in Figure 16. The stability of the oxide in the base cream was further studied using XRD spectrum analysis after exposure to the atmosphere. Specifically, the XRD spectra of calcium oxide embedded in the base cream was taken over varying times of exposure to air with no significant changes observed (Figure 17).

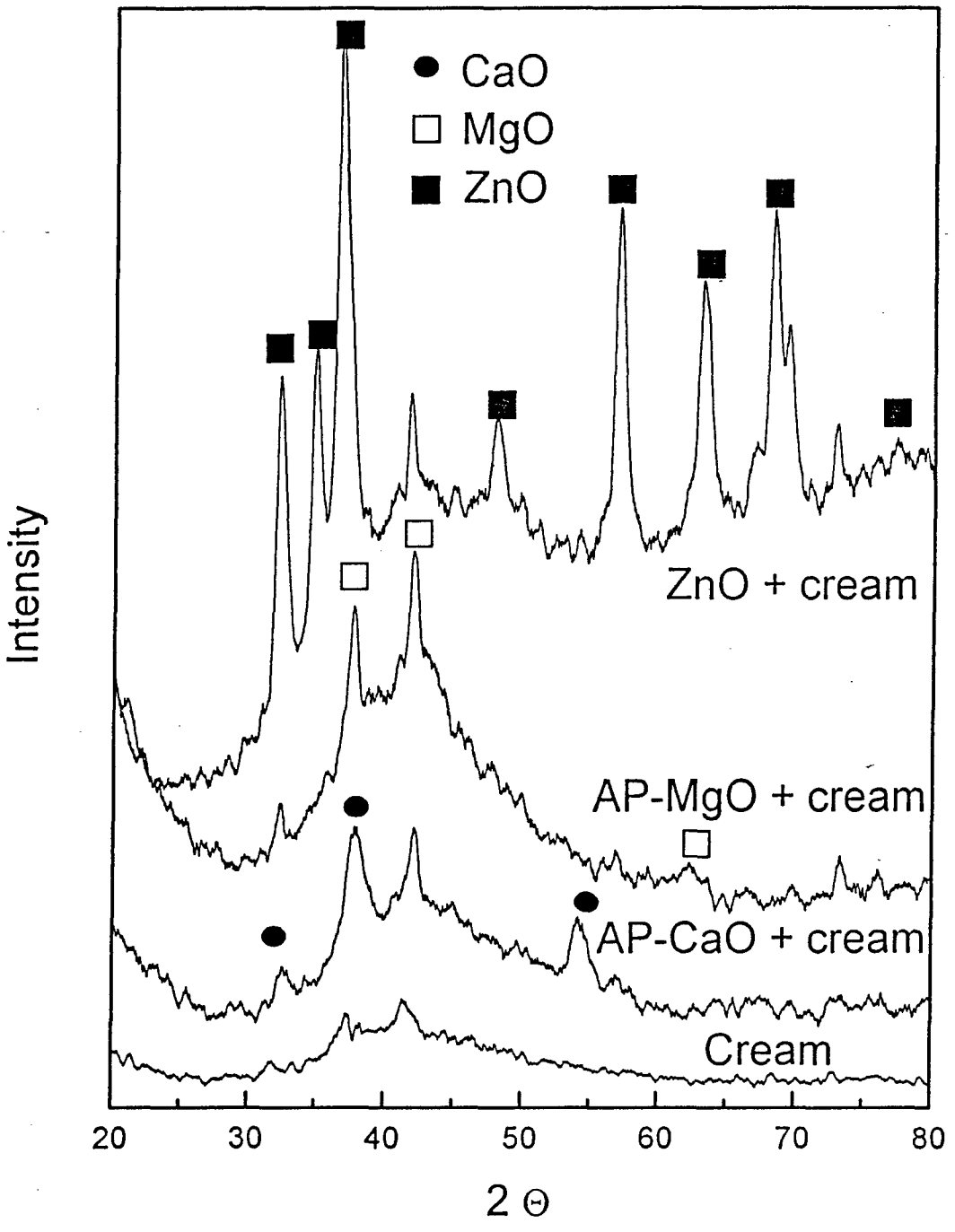

Figure 16. XRD Spectra of a Skin Cream System Composed of Metal Oxides Embedded in the Base Cream

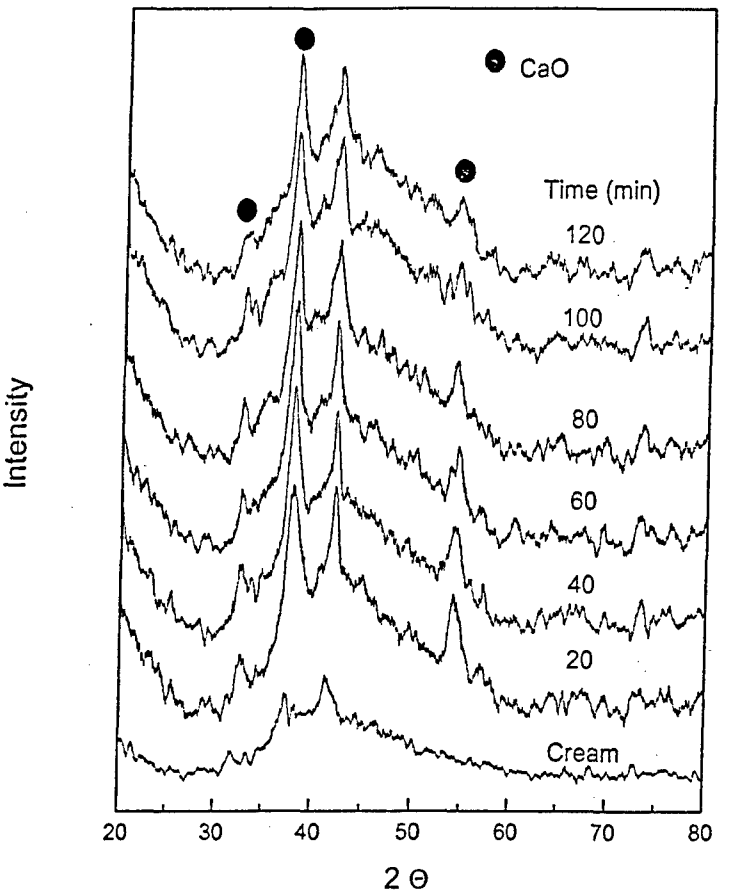

Figure 17. XRD Spectra of AP-CaO Mixed with the Base Cream At Various Times of Exposure to Air

2.4 Preliminary Test Results of Cream/Adsorbent Prototype Systems

Prototype skin topical protectant systems were prepared using AP-MgO as the active ingredient. Preliminary tests using Nantek's paraoxon and 2-CEES test procedures were conducted with the following results. For the paraoxon studies, 0.1 g of AP-MgO was incorporated into approximately 1.5 g of the base cream provided by the Army Medical Research Office. When paraoxon was added to the reaction flask (containing the cream mixed with a freshly distilled solvent), a color change was observed from white to yellow (similar to the results obtained during reaction with the adsorbents alone). This is a good indication that the paraoxon was able to penetrate the cream layer and some reaction likely took place. As discussed earlier, the yellow color is believed to be due to the nitrophenol anion, a decomposition product that is subsequently back-adsorbed onto the metal oxide surface.

As expected, the rate of the reaction was slower when reactants were embedded in the base cream. Nevertheless, a decrease in the paraoxon peak intensity was observed (refer to Table VI). The chemical analysis techniques utilized had sufficient noise in the response that work will be needed to better quantify the mimic reaction with the cream/adsorbent systems. Also, additional experiments need to be developed to eliminate the solvent from the reaction. In current experiments, the reaction is studied using a UV-Vis spectrophotometer with paraoxon dissolved in the solvent as the starting material and p-nitrophenol as the product of reaction. Such gas-phase measurements of paraoxon alone using this method are not possible due to its low vapor pressure. The solvent, however, did not appear to dissolve any of the base cream.

Preliminary test results for the destructive adsorption of the mustard mimic, 2-CEES, were also very encouraging. As with paraoxon, the adsorbent/cream mixture reacted with the mimic albeit at a slower rate

than observed during the earlier adsorbent studies. It is believed that the cream is forming a barrier for the nerve agents, thus slowing the availability of the mimic to the adsorbent surface sites. Refer to Figure 18 for the comparison of the formation of the decomposition product, ethylvinyl sulfide, for calcium and magnesium oxides adsorbents with and without the addition of the base cream.

Table VI. Preliminary Paraoxon (4.5μL) Test Results for AP-MgO/Cream Prototype Systems

Sample	% Paraoxon adsorbed after 2 hours	% Paraoxon adsorbed after 20 hours
AP-MgO/pentane	100%	100%
AP-MgO/cream/pentane	17%	40%
AP-MgO/cream/THF	5%	21%
AP-MgO/cream/toluene	100%	100%

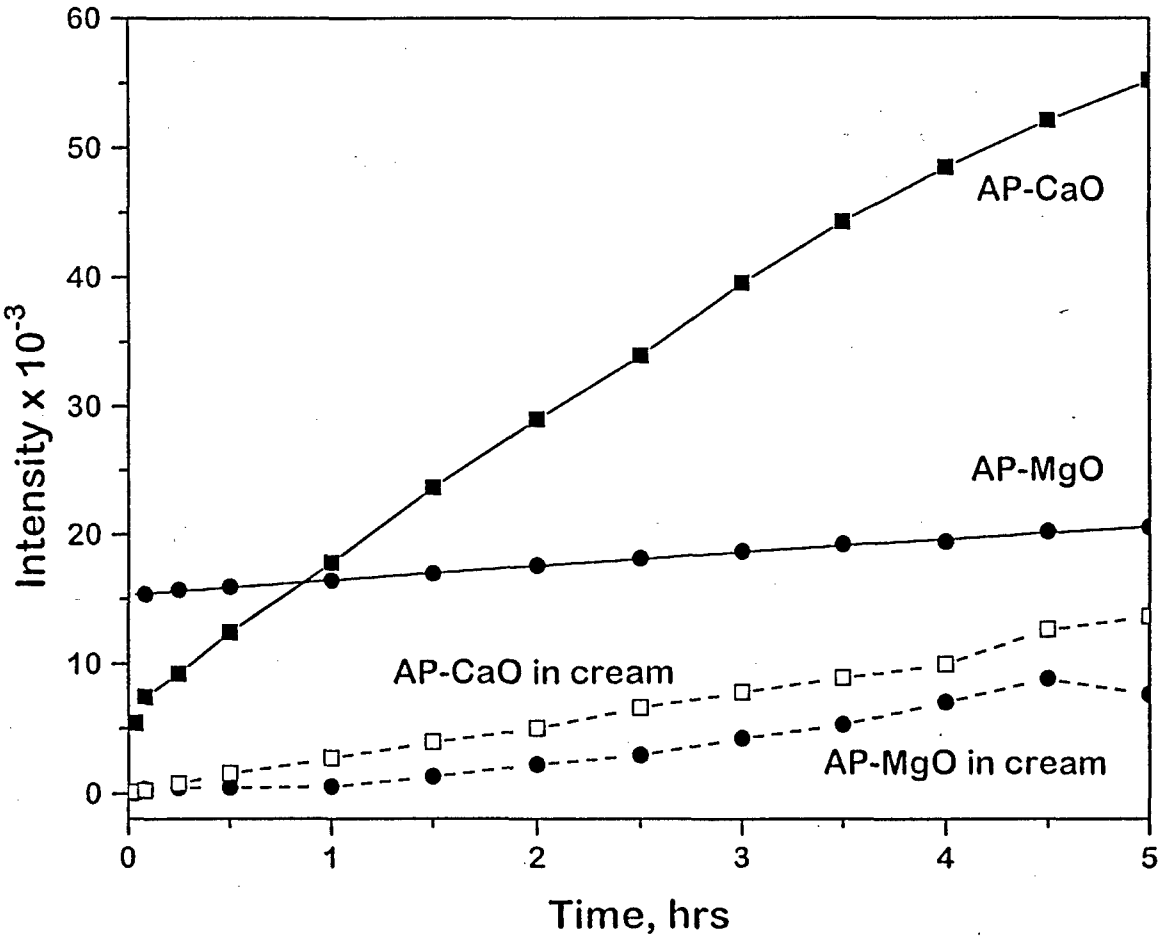

Figure 18. Appearance of Ethylvinyl Sulfide During the Mustard Mimic, 2-CEES, Reaction with on Metal Oxides With and Without the Base Cream

2.5. Calibration Studies with Actual Nerve Agents

During the Phase I Research, Nantek worked with the Midwest Research Institute (MRI) in Kansas City, Missouri, to calibrate the performance of AP-MgO and [Fe_2O_3]AP-CaO with actual nerve agent (VX) and mustard (HD). The overall objective of the work was to confirm the destructive performance of Nantek's most efficient reactive nanoparticle adsorbents. Depending on the nature of the results, a calibration of the performance of the reactive adsorbents with mimics and actual nerve agents were to be conducted. These limited tests are intended to provide a preliminary comparative basis of DAT with mimics and real chemical agents. Real agents are expected to be much more reactive than the mimics, and work with mimics is expected to understate true performance. However, this expectation must be confirmed. Within the budget constraints, only limited tests were conducted using two of Nantek's most reactive adsorbents and two military agent. A brief summary of the findings is provided below. Appendix A provides a copy of the final test report from Donna Nichols of MRI.

Both the VX and HD tests followed the same experimental protocol. Namely, 0.1 g of AP-MgO or [Fe_2O_3]AP-CaO was weighed and placed in an Erlenmeyer flask and covered with parafilm (several flasks were prepared at the same time). Then, 100 mL of pentane was added to each flask. Thereupon 4 or 20 μL of VX (or HD) was added and the start time recorded. After two hours, a 100 μL sample was removed, diluted to 1 mL with 900 μL of pentane, and analysis for VX (or HD) was carried out by Gas Chromatography with a Flame Photoionization Detector (GC/FPD) especially set for sulfur detection. Samples were also extracted after 6 hours and analyzed.

After 6 hours, much of the excess pentane was decanted into a storage container. With flow of nitrogen, the remaining pentane was driven off. 100 mL of methylene chloride, CH_2Cl_2, was added to the used nanoparticle reactant and the sample was sonicated for 15 minutes. The sample was then centrifuged for 10 minutes in two 500 mL centrifuge tubes. The CH_2Cl_2 solvent was then decanted into storage containers. After dilution of the 100 μL samples to 1 mL by adding 900 μL of pure CH_2Cl_2, the sample was analyzed by GC/FPD.

Nantek's AP-MgO destructively adsorbed the VX completely for both the 4 μL and 20 μL loadings. No VX was extracted from the used AP-MgO sample using CH_2Cl_2 as an extraction solvent. Nantek's [Fe_2O_3]AP-CaO reactant also completely adsorbed 4 μL of VX; however, when 20 μL was used, about 60% of the VX remained after 6 hours.

For the HD experiments, two methods were used: (1) the same method as described above for VX, and (2) a dry method where 4 μL of HD was injected directly onto dry AP-MgO or [Fe_2O_3]AP-CaO. After 6 hours, the used AP-MgO or [Fe_2O_3]AP-CaO was extracted with CH_2Cl_2, and analysis for HD was carried out by FID Gas Chromatography. These experiments indicated that some of the HD has been adsorbed/destroyed, but not all. The AP-MgO behaved best with about 50% decomposition within 6 hours. However, the HD experiments were somewhat inconclusive due to wide variability and significant analytical noise. Note that the control (measurement of the % of HD present with no addition of the oxide ranged from 75% to 125% for the four test trials conducted).

These studies, however, demonstrate two important things: (1) Better formulations of nanoparticle metal oxides are needed for HD decomposition, although AP-MgO behaved exceptionally well for VX destructive adsorption; and (2) Based on comparative studies, the mimics we have chosen, namely paraoxon and 2-CEES, proved to be good mimics for modeling the destructive adsorption eaction with the VX and HD military agents. In fact, paraoxon and VX destructive adsorption tracked very well with each other for 4 μL and 20 μL tests. In addition, recent work on 2-CEES has shown that results are similar to HD; that is partial (85%) destruction over 6 hours was observed.

It should be emphasized that for these initial tests comparatively large amounts of mimics or military nerve agents were used. These are very demanding tests, and the fact that some HD was not destroyed should not be discouraging. Further research on new, more reactive, nanoparticle formulations as well as using more realistic ratios of mimics or agents to adsorbent needs to be carried out.

3.0 CONCLUSIONS AND MAJOR FINDINGS OF THE RESEARCH

A broad series of nanoscale metal oxides as well as activated carbon have been studied for destructive adsorbance during the Phase I Research effort. The following represents the major findings of the Phase I Research.

3.1 Identification of Suitable Nanoscale Reactive Adsorbent Materials

The best formulations appear to be AP-MgO, [Fe_2O_3]AP-CaO, [ZnO]AP-MgO, and CP-CaO. At this time AP-MgO alone or in combination with a different metal oxide coating appears to be the most suitable reactive adsorbent for the topical skin cream application. However, substantial work is still needed to understand the products of the reaction, to custom design the most reactive adsorbent, and to incrementally improve the reaction kinetics, especially to improve performance with HD.

Based on the preliminary paraoxon and 2-CEES decomposition studies, iron oxide coated CaO, coated and uncoated AP-MgO and high surface area ZnO provide significant promise for a reactive adsorbent in the skin-protectant application. The Fe_2O_3 coating provides enhanced reaction possibly due to a catalytic effect and/or due to the prevention of hydroxylation of the oxide powders. Composite samples prepared of high surface area magnesium or calcium oxide coated with a layer of high surface area zinc oxide could be strong candidates for this application. The ZnO layer should further prevent the hydrolysis of the oxide. This technique effectively expands the surface area of the ZnO with the underlying magnesium or calcium structure providing a high surface area substrate. Recall from the earlier section, that [ZnO]AP-MgO materials were synthesized with a surface area of 165 m^2/g. This surface area achieved was nearly 7 times larger than commercially available materials. More importantly, paraoxon was completely destroyed within two minutes of exposure to the special zinc composite material while commercial ZnO powders exhibited only modest reactivity after 20 hours of exposure (refer to Figure 2).

As discussed previously, the enhancing effect of the outer metal oxide coating (the shell material of these core/shell nanoparticles), could be due to a catalytic effect where the outer oxide shuttles fragments of the mimic into the core oxide, where it is consumed. This catalytic effect has been clearly demonstrated in high temperature (400-500°C) destructive adsorption work, but now appears to possibly be viable at room temperature as well. Further work to delineate the true function of the shell oxide (catalytic shuttle or protectant against hydrolysis or some other subtle effect) will be carried out during the Phase II Research. Additional new formulations will be synthesized so that larger surface areas are generated and specific chemical advantages are leveraged [e.g. [CaO]Ap-MgO (higher basicity); [ZnO]AP-MgO (resistance to hydrolysis); [V_2O_5]AP-MgO (superior catalytic enhancement)].

Autoclave-prepared MgO samples showed remarkable performance. These particles are the highest surface area samples tested, with a surface area of over 500 m^2/g. For the paraoxon studies, the AP-MgO nearly instantaneously destructively adsorbed all of the paraoxon before the first reading at two minutes after exposure. For the 2-CEES studies, it appears that the oxide reached a rapid equilibrium in less than five minutes where much of the 2-CEES was destroyed, but the ethylvinyl sulfide was also absorbed on the particle surface. This result shows the need to develop additional tests suited for the case where rapid adsorption of both the starting material and products of reaction occurs. In addition, the solid samples of reacted AP-MgO were studied and significant evidence of reaction or destructive adsorption of the paraoxon was observed.

3.2 Comparison of Nanoscale Reactive Particles with Activated Carbon

While evidence of actual destruction of the mimic compound was observed for many of Nantek's custom reactive adsorbents, we were able to confirm that destructive adsorption does not take place using activated carbon, a well known highly adsorbent material. Activated carbon seems to quickly adsorb both paraoxon and 2-CEES; however, no evidence of decomposition of the mimic compounds was observed. An unexpected outcome of the research was that activated carbon actually has a lower adsorption capacity than Nantek's AP-MgO material on an equivalent gram basis. When 0.1 g of each adsorbent were used, only 4.5 μL of paraoxon was completely adsorbed on the activated carbon surface whereas the AP-MgO adsorbed/destroyed 20 μL of paraoxon.

3.3 New Synthesis Breakthroughs for the Production of High Surface Area Zinc Oxide

A tremendous amount of effort during the Phase I Research was focused on the development of novel zinc oxide nanoscale materials that demonstrated excellent capacity for decomposition of the military agent mimics. As discussed above and in the previous sections, Nantek's standard aerogel synthesis procedures were not appropriate for the production of zinc oxide powders since zinc does not react with methanol to produce zinc methoxide, a critical step for standard aerogel synthesis. Through a thorough review of the state-of-art and much experimentation, synthesis approaches were developed that yielded highly reactive zinc oxide material with a surface area approximately 3 times that of commercially available "high" surface area ZnO powders. In an attempt to even further expand the reactive capacity of the zinc oxide material, custom design and synthesis of [ZnO]AP-MgO nanocrystals were preliminarily conducted. The surface area achieved for these custom composite materials was nearly 7 times larger than commercially available zinc oxide powders. More importantly, paraoxon was completely destroyed within two minutes of exposure to the special zinc composite material while commercial zinc oxide powders exhibited only modest reactivity after 20 hours of exposure (refer to Figure 2).

3.4 Decomposition of the Military Nerve Agents, VX and HD

Nantek's AP-MgO showed exceptional results for the destruction of VX with complete decomposition for both 4 μL and 20 μL loadings. In addition, no VX was extracted from the used AP-MgO sample using CH_2Cl_2 as an extraction solvent. Nantek's $[Fe_2O_3]$AP-CaO reactant also completely adsorbed 4 μL of VX; however, when 20 μL was used, about 60% of the VX remained after 6 hours. The HD experiments indicated that some of the HD is adsorbed upon contact with the nanoscale reactants, but not all. AP-MgO behaved the best destroying approximately 50% of the agent. Considerable analytical uncertainty was present during the GC studies as demonstrated by a wide range of data for the control test which measures the amount of HD present without the addition of the reactant. This control varied from 75% to 125% in the four test trials. Such difficulties suggest the need to develop better analytical techniques for the measurement of decomposition of the mustard agent.

Two important conclusions, however, can be drawn from the nerve agent testing: (1) Better formulations of nanoparticle metal oxides are needed for HD decomposition, although AP-MgO behaved exceptionally well for VX destructive adsorption; and (2) The mimics selected, paraoxon and 2-CEES, provide a strongly correlated reaction model for the decomposition of VX and HD, respectively.

3.5 Chemical Compatibility of the Adsorbents with the Base Cream

Several nanoscale metal oxide samples including magnesium, calcium and zinc demonstrated compatibility upon mixing with the base cream provided by the Army. Furthermore, no significant changes in the cream were observed using XRD analysis upon prolonged exposure to atmospheric conditions.

3.6 Decomposition of Mimics Upon Exposure to the Prototype Skin Cream Systems

In the preliminary Phase I Research tests, AP-MgO appears to remain reactive upon mixing with the base cream for both paraoxon and 2-CEES exposure. Due to the barrier nature of the base cream, the reaction occurred at a slower rate than observed when the reactants were directly exposed to the mimic compounds.

References

1. a. Li, Y. X.; Klabunde, K. J. *Langmuir* **1991**, *7*, 1388.
   b. Li, Y. X.; Schlup, J. R.; Klabunde, K. J. *Langmuir* **1991**, *7*, 1394.
2. Ekerdt, J. G.; Klabunde, K. J.; Shapley, J. R.; White, J. M.; Yates, Jr., J. T. *J. Phys. Chem.* **1988**, *92*, 6182.
3. Tzou, T. Z.; Weller, S. W. Unpublished paper (private communication in 1991).
4. Baier, R. W.; Weller, S. W. *In. Eng. Chem. Process Des. Dev.* **1967**, *6*, 380.
5. Graven, W. M.; Weller, S. W.; Peters, D. L. *Ind. Eng. Chem. Process Des. Dev.* **1966,** *5*, 183.
6. Parfitt, R. L.; Russell, J. D. *J. Soil Sci.* **1977**, *28*, 297.
7. Lyklema, L. *Environ. Sci. Technol.* **1980**, *14*, 297.
8. Strumm, W.; Furrer, G.; Kunz, B. *Croat. Chem. Acta* **1983**, 585.
9. Graven, W. M.; Paton, J. D.; Weller, S. W. *Ind. Eng. Chem. Process Des. Dev.* **1966**, *5*, 34.
10. Smentkowski, V. S.; Hagans, P. L.; Yates, Jr., J. T. *J. Phys. Chem.* **1988**, *92*, 6352.
11. Smentkowski, V. S.; Hagans, P. L.; Yates, Jr., J. T. U. S. Patent No. 4,871,526.
12. Guo, X.; Yoshinobu, J.; Yates, Jr., J. T. *J. Phys. Chem.* **1990**, *94*, 6839.
13. Dulcey, C. S.; Lin, M. C.; Hsu, C. C. *Chem. Phys. Lett.* **1985**, *115*, 481.
14. Hegde, R. I.; Greenlief, C. M.; White, J. M. *J. Phys. Chem.* **1985**, *89*, 2886.
15. Henderson, M. A.; White, J. M. *J. Phys. Chem.* **1988**, *110*, 6939.
16. Hegde, R. I.; White, J. M. *Appl. Surf. Sci.* **1987**, *28*, 1.
17. Henderson, M. A.; Jin, T.; White, J. M. *J. Phys. Chem.* **1986**, *90*, 4607.
18. Templeton, M. K.; Weinberg, W. H. *J. Am. Chem. Soc.* **1985**, *107*, 97.
19. Templeton, M. K.; Weinberg, W. H. *J. Am. Chem Soc.* **1985**, *107*, 774.
20. Kuiper, A. E. T.; van Bokhoven, J. J. G. M.; Medema, J. *J. Catal.* **1976**, *43*, 154.
21. Li, Y. X.; Koper, O.; Atteya, M.; Klabunde, K. J. *Chem of Mater.*, **1992**, *4*, 323.
22. a. Lin, S. T.; Klabunde, K. J. *Langmuir* **1985**, *1*, 600.
    b. Klabunde, K. J.; Matsuhashi, H. *J. Am. Chem. Soc.* **1987**, *109*, 1111.
    c. Klabunde, K. J.; Hoq, M. F.; Mousa, F.; Matsuhashi, H. *Preparative Chemistry Using Supported Reagents*, Laszlo, P., Ed.; Academic: New York, 1987, p. 35.
    d. Nieves, I.; Klabunde, K. J. *Mater. Chem. Phys.* **1988**, *18*, 485.
    e. Utampanya, S.; Klabunde, K. H.; Schlup, J. R. *Chem. Mater.* **1991**, *3*, 175.
    f. Atteya, M.; Klabunde, K. J. *Chem. Mater.* **1991**, *3*, 182.
23. "Metal Oxide Particles: Detoxification of Nerve Gases", T. Collins, A. Held, R. Rainbolt, Chemical Engineering System Design 2, W. Walawender (Professor), May 1993, 40 pages.
24. Klabunde, K. J.; Khaleel, A.; Park, D. *High Temp. and Materials Science*, **1995,** *33*, 99-106.
25. Klabunde, K.J.; Stark, J.; Koper, O.; Mohs, C.; Park, D.G.; Decker, S.; Jiang, Yi; Lagadic, I.; Zhang, D.; J. Physical Chemistry, **1996**, *100*, 12142-12153 (invited feature article).
26. Yang, Y. C., J. A. baker, J. R. Ward, *Chem. Rev.*,**1992**, *92*, 1729-1743.
27. N.S. Gajbhiye, U. Bhattacharya, V.S. Darshane, *Thermochimica Acta*, **1995**, *264*, 219-230.
28. Goel, S.C., Chiang, M.Y., Gibbons, P.C., Buhro, W.E., *Mat. Res. Soc. Symp. Proc.*, **1992**, *271*, 3-13.

29. Ohyama, M., Kozuka, H., Yoko, K., Sakka, S., *J. Ceramic Soc. of Japan*, **1996**, *104*, 296-300.
30. Spanhel, L., Anderson, M.A., *J. Am. Chem. Soc.*, **1991**, *113*, 2826-2833.
31. Sakohara, S., Tickanen, L.D., Anderson, M.A., *J. Phys. Chem.*, **1992**, *96*, 11086-11091.
32. Lauf, R., Bond, W.D., *Ceramic Bulletin*, **1984**, *63*, 278-281.
33. Heistand, R.H., Chia, Y.H., *Mat. Res. Soc. Symp. Proc.*, **1993**, *73*, 93-98.
34. Burlitch, J.M., Hayes, S. E., Whitwell, G.E., *Organometallics*, **1982**, *1*, 1074-1083.
35. Fujita, S., Usui, M., Ito, H., Takezawa, N., *J. Catal.*, **1995**, *157*, 403-413.
36. Ruixia, L., Peiying, W., Shiliang, W., *Varistor Tech.*, 117-120.
37. Spanhel, L., *Eurogel '91 Proc.*, **1992**, 407-414.
38. Lakeman, C.D.E., Payne, D.A., *Mat. Chem. Phys.*, **1994**, *38*, 305-324.
39. Unger, B., Popp, P., Schade, U., Hahnert, M., *J. Non-Cryst.Solids*, **1993**, *160*, 152-161.
40. Decker, S., Klabunde K.J., *J. Am. Chem. Soc.*, **1996**, *118*, 12465-12466.
41. Jiang Y., Decker S., Klabunde, K.J., unpublished work.

APPENDIX A

MIDWEST RESEARCH INSTITUTE FINAL REPORT

MIDWEST RESEARCH INSTITUTE
425 Volker Boulevard
Kansas City, Missouri 64110
Telephone (816) 753-7600
Telefax (816) 753-8420

June 6, 1997

Dr. Kenneth Klabunde
Nantek, Inc.
1500 Hayes Drive
Manhattan, KS 66502

Subject: Final Report, MRI Project No. 4732, "Testing of Metal Oxide Powders for Chemical Agent Destruction"

Dear Dr. Klabunde:

Introduction

The objective of this study was to determine the effects, if any, that certain high surface oxide powders have on the chemical agents HD and VX. The scope of the work included the use of several oxides, adding neat agent to them and determining the residual agent by use of gas chromatography. Through this analysis predictions could be made on the ability of these oxides to protect or bind up such agents.

The experiments performed included spiking solutions of pentane and magnesium oxide (MgO) and solutions of pentane and iron oxide (Fe_2O_3) with VX. The oxides were supplied by Nantek Affiliates. Aliquots were taken at certain time intervals and analyzed. The spent oxides were then extracted with methylene chloride to determine if any of the agent was tied up within the powders. HD experiments spiked directly onto magnesium oxide and iron oxide. These were allowed to react. Then the oxides were extracted with methylene chloride and analyzed.

Changes in the original test method were made after initial results showed the HD experiment may not be working. The experiments were changed to provide a more enclosed environment for the oxides to react with the agent. Discussions with Nantek affiliates suggested adding HD to the oxides instead of to the solution of pentane and the oxides.

Experiments

Original experiments began with adding 4 μL of neat HD to a mixture of 100 mL of pentane and 100 mg of MgO in an Erlenmeyer flask, in duplicate. Quality control consisted of a method blank (pentane with MgO), a lab control (pentane only), and a lab control spike (pentane spiked with 4 μL of HD). The flasks were placed on stir plates and allowed to stir for 2 minutes, 2 hours, and 6 hours, approximately. At each time interval a 100-μL aliquot was removed and added to 900 μL of pentane and analyzed by GC/FPD in sulfur mode. The pentane was decanted and the oxide dried with a slow stream of nitrogen. The spent oxide was then extracted with 100 mL of methylene chloride. Dilutions were made and run by GC/FPD. This initial experiment allowed the determination of any problems or unforeseen circumstances.

At this time changes made to the test method for HD included spiking the HD directly onto the oxide and use of Erlenmeyer flask with stoppers to reduce risk of evaporation of solvent. The experiment that is reported was done in the following manner. The 4 μL of HD was spiked directly onto the oxide in Erlenmeyer flask with stoppers. Both the MgO and Fe_2O_3 were tested. QC remained the same except that method blanks were prepared for each of the oxides. The samples were allowed to react for approximately 6 hours. At the end of the reaction period 100 mL of methylene chloride was added to the flasks. The flasks were placed into a sonic bath and extracted for 15 minutes. The samples containing oxides were split into two 50-mL centrifuge tubes and centrifuged for approximately 10 minutes. The extracts were then combined into a single labeled storage container. Aliquots (100 μL) of each of the samples were placed into autosampler vials with 900 μL of methylene chloride for analysis. Analysis was done by GC/FPD in sulfur mode.

Experiments for the degradation of VX were performed according to the scope of work. A 100-mg amount of each oxide (MgO and Fe_2O_3) was weighed into individual Erlenmeyer flasks, and100 mL of pentane was immediately added to each flask, in duplicate samples. Quality control consisted of a method blank (oxide and pentane), laboratory control (pentane only), and a laboratory control spike (pentane and VX). The samples and the laboratory control spike were spiked with the appropriate amount of VX.

Experiments with VX included 4-μL spikes onto each of the oxides (MgO and Fe_2O_3) and 20-μL spikes onto each of the oxides. At 2-hour and 6-hour time intervals aliquots of the samples were taken for analysis. The following dilution scheme was used to bring the samples within the range of the curve. For the 4-μL samples, 100 μL of sample was added to 900 μL of pentane, and for the 20-μL samples 100 μL was added to 9.9mL of pentane. The dilutions were analyzed by GC/FPD in phosphorous mode. At the end of the 6-hour time interval the pentane was decanted off and the oxide was dried under a slow stream of nitrogen gas. The spent oxides were then extracted for 15 minutes in a sonic bath with 100 mL of methylene chloride. The samples containing oxides had to be centrifuged for approximately 10 minutes. Each of the extracts was decanted into the

properly labeled storage container. The dilution scheme for the original samples was repeated and analyzed by GC/FPD in phosphorous mode.

Results

The effects of the oxides on 4μL of HD were relatively minimal. After 6 hours on the MgO over 50% of the HD still remained, and after 6 hours on the Fe_2O_3 over 75% of the HD remained. Figures 2 through 5 (see Attachment) demonstrate the residual HD. Table 1 shows the individual results of each of the samples prepared for the HD experiment. The lab control spike had recovery well within acceptable parameters of 75-125%.

Table 1. HD (4 μL) on MgO and Fe_2O_3

HD Sample ID	2 Hour Extraction Recovery (μg/mL)	Amount of HD[a] Remaining (%)
Method Blank 100 mg MgO F037-MB-MgO	ND, < 0.2 μg/mL[b]	ND, < 0.2 μg/mL
Method Blank 100 mg Fe_2O_3 F037-MB-FeO	ND, < 0.2 μg/mL	ND, < 0.2 μg/mL
Lab Control No Oxide, No Spike F037-LC	ND, < 0.2 μg/mL	ND, < 0.2 μg/mL
Lab Control Spike No Oxide, 4 μL HD F037-LCS	4.84 μg/mL	95.3%
Sample 1 - MgO 100 mg MgO, 4 μL HD F037-1-MgO	3.45 μg/mL	67.9%
Sample 2 - MgO 100 mg MgO, 4 μL HD F037-2-MgO	2.86 μg/mL	56.3%
Sample 1 - FeO 100 mg Fe_2O_3, 4 μL HD F037-1-FeO	4.13 μg/mL	81.3%
Sample 2 - FeO 100 mg Fe_2O_3, 4 μL HD F037-2-FeO	3.93 μg/mL	77.4%

[a] % Recovery: % = 100 x (conc. found/conc. expected). 100% = 5.08 μg/mL

[b] ND: Not detected above curve low point. The limit of detection for this analysis was set at the lowest point of the calibration curve (0.2 μg/mL).

The effects of the oxides on VX were more substantial. The 4-μL spike into the MgO solution showed complete binding of the agent; see Figure 7. Table 2 gives the individual results for each of the samples. Although the lab control spike is below 75% recovery, the relative standard deviation (RSD) between the two sampling periods is low.

Table 2. VX (4 μL) on MgO

VX Sample ID	2 Hour Recovery (μg/mL)	Amount of VX Remaining[a] (%)	6 Hour Recovery (μg/mL)	Amount of VX Remaining (%)	$MeCl_2$ Recovery (μg/mL)
Method Blank 100 mg MgO E127-MB	ND,[b] < 0.5 μg/mL	ND, < 0.5 μg/mL	ND, < 0.5 μg/mL	ND, < 0.5 μg/mL	ND, < 0.5 μg/mL
Lab Control no MgO, no spike E127-LC	0.74 μg/mL Contamination		ND, < 0.5 μg/mL	ND, < 0.5 μg/mL	ND, < 0.5 μg/mL
Lab Control Spike no MgO, 4 μL VX E127-LCS	2.68 μg/mL	66.3%	2.75 μg/mL	68.1%	ND, < 0.5 μg/mL
Sample 1 100 mg MgO, 4 μL VX E127-1	ND, < 0.5 μg/mL	ND, < 0.5 μg/mL	ND, < 0.5 μg/mL	ND, < 0.5 μg/mL	ND, < 0.5 μg/mL
Sample 2 100 mg MgO, 4 μL VX E127-2	ND, < 0.5 μg/mL	ND, < 0.5 μg/mL	ND, < 0.5 μg/mL	ND, < 0.5 μg/mL	ND, < 0.5 μg/mL

[a] % Recovery: % = 100 x (conc. found/conc. expected). 100% = 4.04 μg/mL
[b] ND: Not detected above curve low point. The limit of detection for this analysis was set at the lowest point of the calibration curve (0.5 μg/mL).

The 20-μL VX spike into the MgO solution also showed the efficiency of the MgO to bind up the agent. Figure 8 demonstrates this effect. Table 3 gives the individual results for each of the samples. Again the lab control spike is below 75%, but results between the 2-hour sample and 6-hour sample are consistent.

Table 3. VX (20 µL) on MgO

VX Sample ID	2 Hour Recovery (µg/mL)	Amount Of VX Remaining (%)[a]	6 Hour Recovery (µg/mL)	Amount Of VX Remaining (%)	$MeCl_2$ Recovery (µg/mL)
Method Blank 100 mg MgO E287-MB	ND, < 0.5 µg/mL	ND,[b] < 0.5 µg/mL	ND, < 0.5 µg/mL	ND, < 0.5 µg/mL	ND, < 0.5 µg/mL
Lab Control no MgO, no spike E287-LC	0.67 µg/mL contamination		ND, < 0.5 µg/mL	ND, < 0.5 µg/mL	ND, < 0.5 µg/mL
Lab Control SPIKE no MgO, 20 µL VX E287-LCS	1.42 µg/mL	71.0%	1.3 µg/mL	64.4%	ND, < 0.5 µg/mL
Sample 1 100 mg MgO, 20 µL VX E287-1	0.65 µg/mL	32.2%	ND, < 0.5 µg/mL	ND, < 0.5 µg/mL	ND, < 0.5 µg/mL
Sample 2 100 mg MgO, 20 µL VX E287-2	ND, < 0.5 µg/mL	ND, < 0.5 µg/mL	ND, < 0.5 µg/mL	ND, < 0.5 µg/mL	ND, < 0.5 µg/mL

[a] % Recovery: % = 100 x (conc. found/conc. expected). 100% = 2.02 µg/mL
[b] ND: Not detected above curve low point. The limit of detection for this analysis was set at the lowest point of the calibration curve (0.5 µg/mL).

The Fe_2O_3 solution was not as efficient as the MgO in binding the agent. The 4-µL spike gave favorable results, especially after 6 hours. This can be seen in Figures 9 and 10. The lab control spike was within the acceptable parameters and consistent within the 2-hour sample and the 6-hour sample. However this particular analysis day had several possible contamination problems. In Table 4 the individual sample results reflect possible contamination in the method blank and the 2-hour lab control. The small amounts of agent detected in the samples could also be attributed to this kind of contamination.

Table 4. VX (4 μL) on Fe_2O_3

VX Sample ID	2 Hour Recovery (μg/mL)	Amount of VX Remaining (%)[a]	6 Hour Recovery (μg/mL)	Amount of VX Remaining (%)	$MeCl_2$ Recovery (μg/mL)
Method Blank 100 mg Fe_2O_3 E297-MB	0.49 μg/mL contamination		0.48 μg/mL contamination		ND,[b] < 0.5 μg/mL
Lab Control no Fe_2O_3, no spike E297-LC	0.91 μg/mL contamination		ND, < 0.5 μg/mL	ND, < 0.5 μg/mL	ND, < 0.5 μg/mL
Lab Control Spike no Fe_2O_3, 4 μL VX E297-LCS	3.36 μg/mL	83.4%	3.29 μg/mL	81.6%	ND, < 0.5 μg/mL
Sample 1 100 mg Fe_2O_3, 4 μL VX E297-1	0.5 μg/mL	12.4%	ND, < 0.5 μg/mL	ND, < 0.5 μg/mL	ND, < 0.5 μg/mL
Sample 2 100mg Fe_2O_3, 4 μL VX E297-2	0.48 μg/mL	11.9%	0.49 μg/mL	12.1%	ND, < 0.5 μg/mL

[a] % Recovery: % = 100 x (conc. found/conc. expected). 100% = 4.04 μg/mL

[b] ND: Not detected above curve low point. The limit of detection for this analysis was set at the lowest point of the calibration curve (0.5 μg/mL).

The 20-μL VX spikes in the Fe_2O_3 solution still had significant recoveries after the 6-hour sampling period. Figures 11 through 14 demonstrate the residual agent. Table 5 gives the individual results. The lab control spike has acceptable recovery at both sampling periods. Also, the recoveries on the samples are consistent between the two sampling periods, which would indicate that after 2 hours any decontamination that was going to occur already had.

Table 5. VX (20 µL) on Fe_2O_3

VX Sample ID	2 Hour Recovery (µg/mL)	Amount of VX Remaining (%)[a]	6 Hour Recovery (µg/mL)	Amount of VX Remaining (%)	$MeCl_2$ Recovery (µg/mL)
Method Blank 100 mg Fe_2O_3 E307-MB	ND,[b] < 0.5 µg/mL	ND, < 0.5 µg/mL	ND, < 0.5 µg/mL	ND, < 0.5 µg/mL	ND, < 0.5 µg/mL
Lab Control no Fe_2O_3, no spike E307-LC	ND, < 0.5 µg/mL	ND, < 0.5 µg/mL	ND, < 0.5 µg/mL	ND, < 0.5 µg/mL	ND, < 0.5 µg/mL
Lab Control Spike no Fe_2O_3, 20 µL VX E307-LCS	1.59 µg/mL	78.7%	1.69 µg/mL	83.7%	ND, < 0.5 µg/mL
Sample 1 100 mg Fe_2O_3, 20 µL VX E307-1	1.25 µg/mL	59.4%	1.3 µg/mL	64.4%	ND, < 0.5 µg/mL
Sample 2 100 mg Fe_2O_3, 20 µL VX E307-2	1.29 µg/mL	63.9%	1.23 µg/mL	60.9%	ND, < 0.5 µg/mL

[a] % Recovery: % = 100 x (conc. found/conc. expected). 100% = 2.02 µg/mL

[b] ND: Not detected above curve low point. The limit of detection for this analysis was set at the lowest point of the calibration curve (0.5 µg/mL).

The methylene chloride extractions of the spent oxides showed no recoveries of the agent from the oxides.

Sincerely,

MIDWEST RESEARCH INSTITUTE

Amy M. Richardson
Assistant Chemist

Donna R. Nichols
Senior Chemist

Approved by:

John S. Stanley, Ph.D.
Director
Chemical Sciences Department

Attachment

Chromatogram

Sample Name : CONCAL (3.936ug/mL)
FileName : c:\2700\gc\gc_r\F03A008.raw
Method : F037HD
Start Time : 0.00 min End Time : 8.96 min
Scale Factor: 1.0 Plot Offset: 24 mV

Sample #: 4728-21-8 Page 1 of 1
Date : 6/4/97 11:52 AM
Time of Injection: 6/3/97 06:27 PM
Low Point : 23.81 mV High Point : 582.62 mV
Plot Scale: 558.8 mV

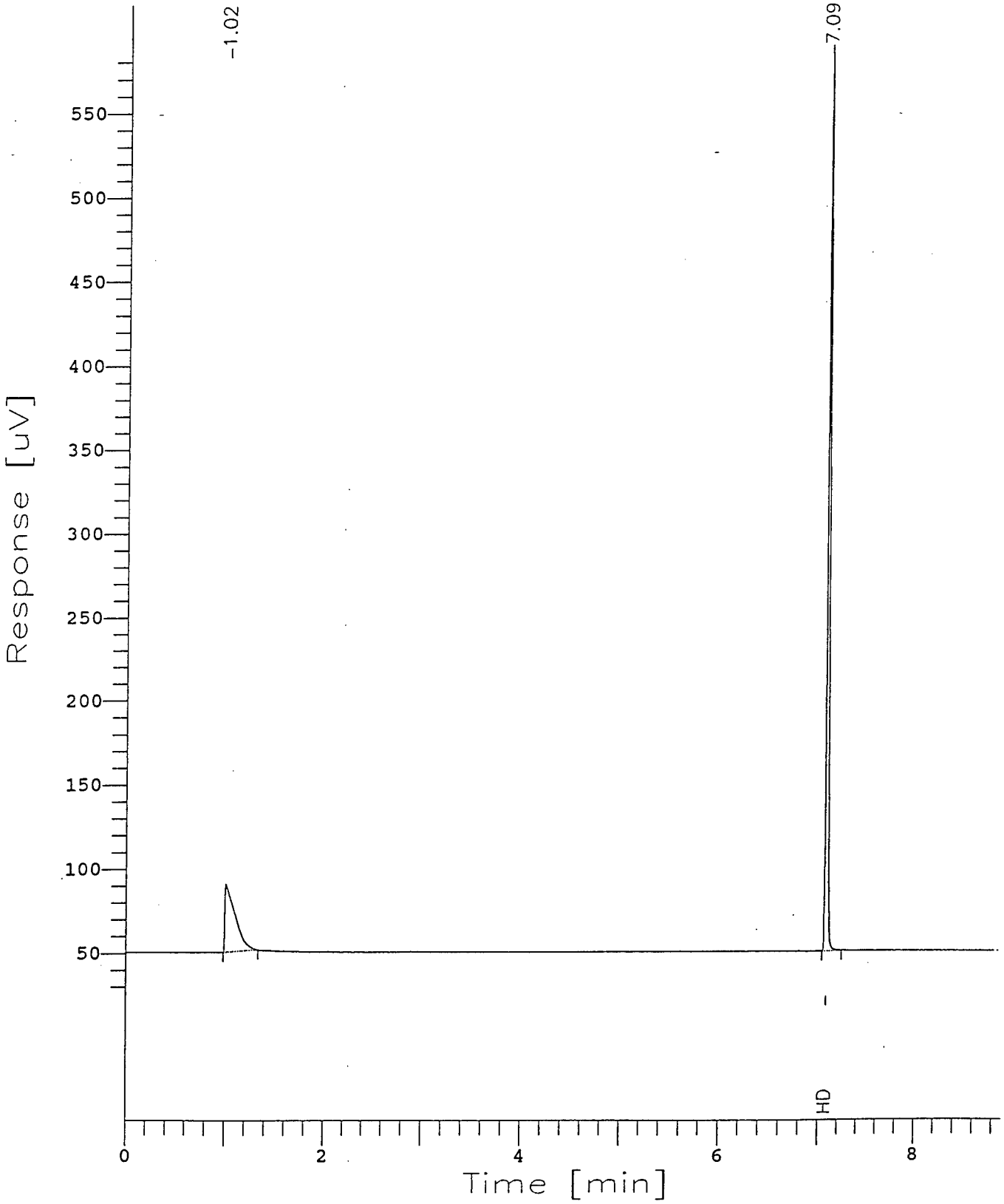

Figure 1. HD Standard (4 µg/mL)

Chromatogram

Sample Name : E037-1-MgO
FileName : c:\2700\gc\gc_r\F03A013.raw
Method : F037HD
Start Time : 0.00 min End Time : 8.96 min
Scale Factor: 1.0 Plot Offset: 33 mV

Sample #: 4uL SPK,OX Page 1 of 1
Date : 6/4/97 11:53 AM
Time of Injection: 6/3/97 07:36 PM
Low Point : 32.50 mV High Point : 409.20 mV
Plot Scale: 376.7 mV

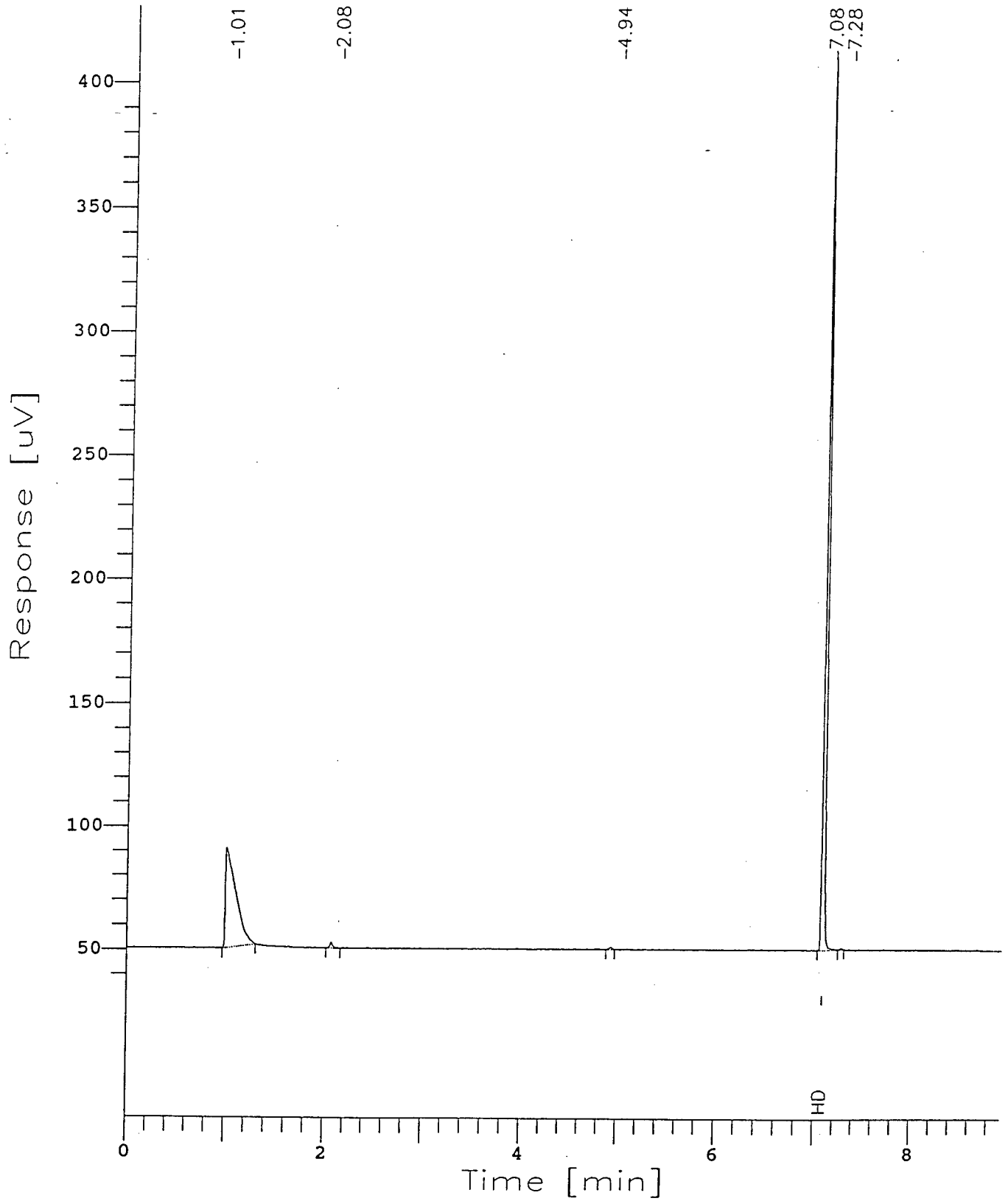

Figure 2. 4 µL HD on MgO, Sample 1 After 6-Hour Extraction

Chromatogram

SampleName : 037-2-MgO
FileName : c:\2700\gc\gc_r\F03A014.raw
Method : F037HD
Start Time : 0.00 min End Time : 8.96 min
Scale Factor: 1.0 Plot Offset: 37 mV

Sample #: 4uL SPK,OX Page 1 of 1
Date : 6/4/97 11:53 AM
Time of Injection: 6/3/97 07:49 PM
Low Point : 37.21 mV High Point : 315.64 mV
Plot Scale: 278.4 mV

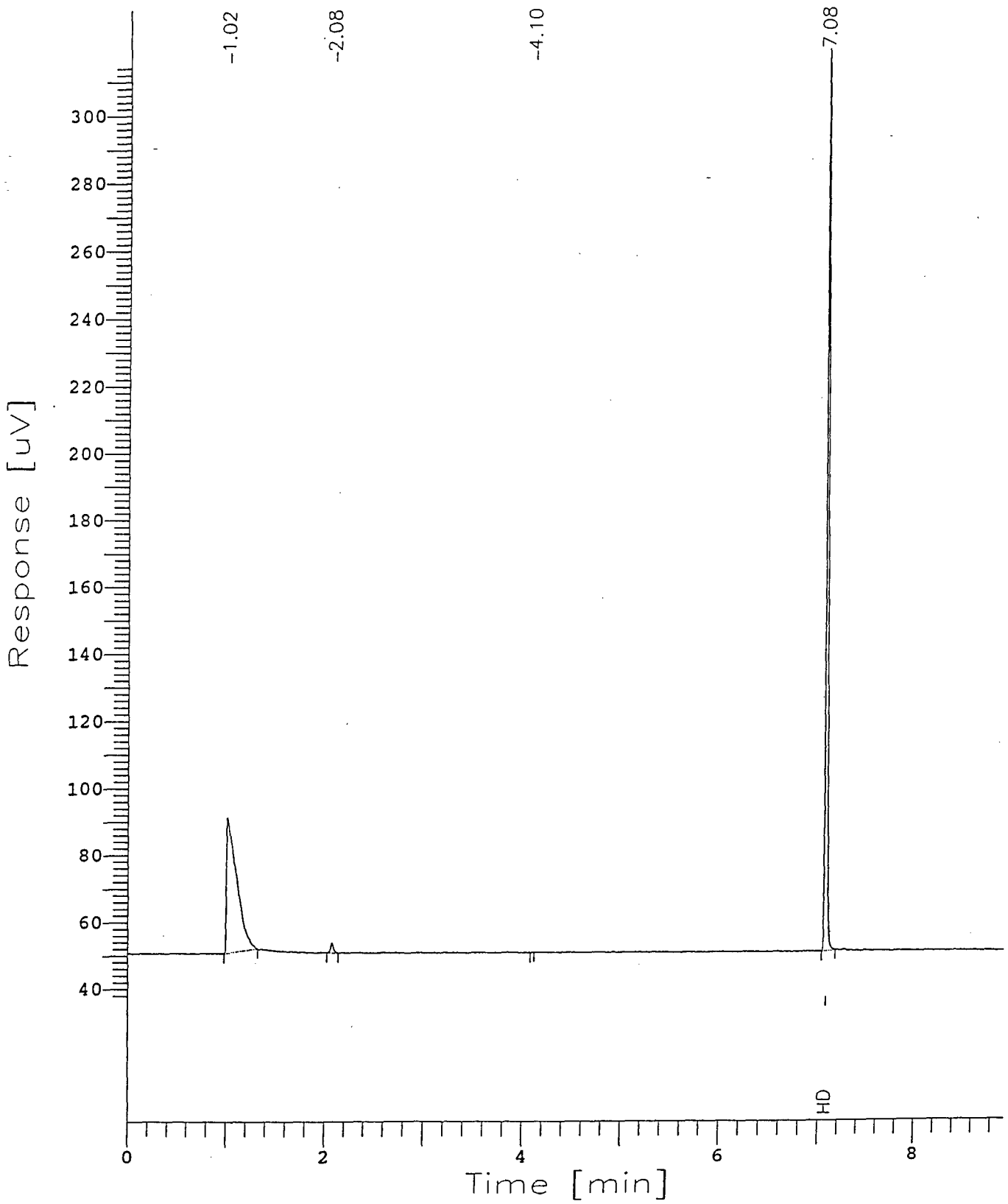

Figure 3. 4 µL HD on MgO, Sample 2 After 6-Hour Extraction

Chromatogram

Sample Name : E037-1-FeO
FileName : c:\2700\gc\gc_r\F03A016.raw
Method : F037HD
Start Time : 0.00 min End Time : 8.96 min
Scale Factor: 1.0 Plot Offset: 27 mV

Sample #: 4uL SPK,OX Page 1 of 1
Date : 6/4/97 11:53 AM
Time of Injection: 6/3/97 08:17 PM
Low Point : 26.90 mV High Point : 522.06 mV
Plot Scale: 495.2 mV

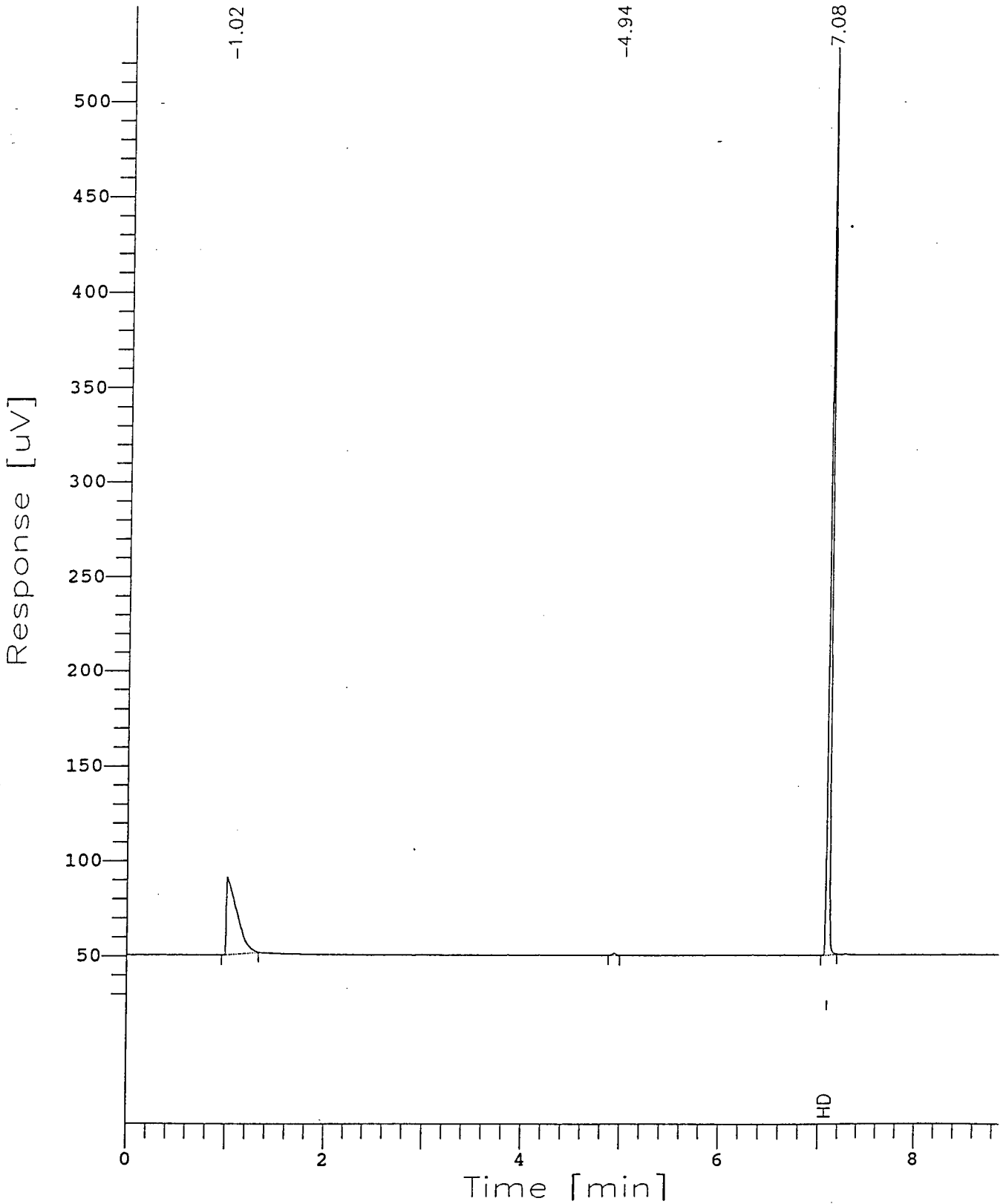

Figure 4. 4 µL HD on Fe_2O_3, Sample 1 After 6-Hour Extraction

Chromatogram

Sample Name : E037-2-FeO
FileName : c:\2700\gc\gc_r\F03A017.raw
Method : F037HD
Start Time : 0.00 min End Time : 8.96 min
Scale Factor: 1.0 Plot Offset: 28 mV

Sample #: 4uL SPK,OX Page 1 of 1
Date : 6/4/97 11:53 AM
Time of Injection: 6/3/97 08:31 PM
Low Point : 27.82 mV High Point : 503.59 mV
Plot Scale: 475.8 mV

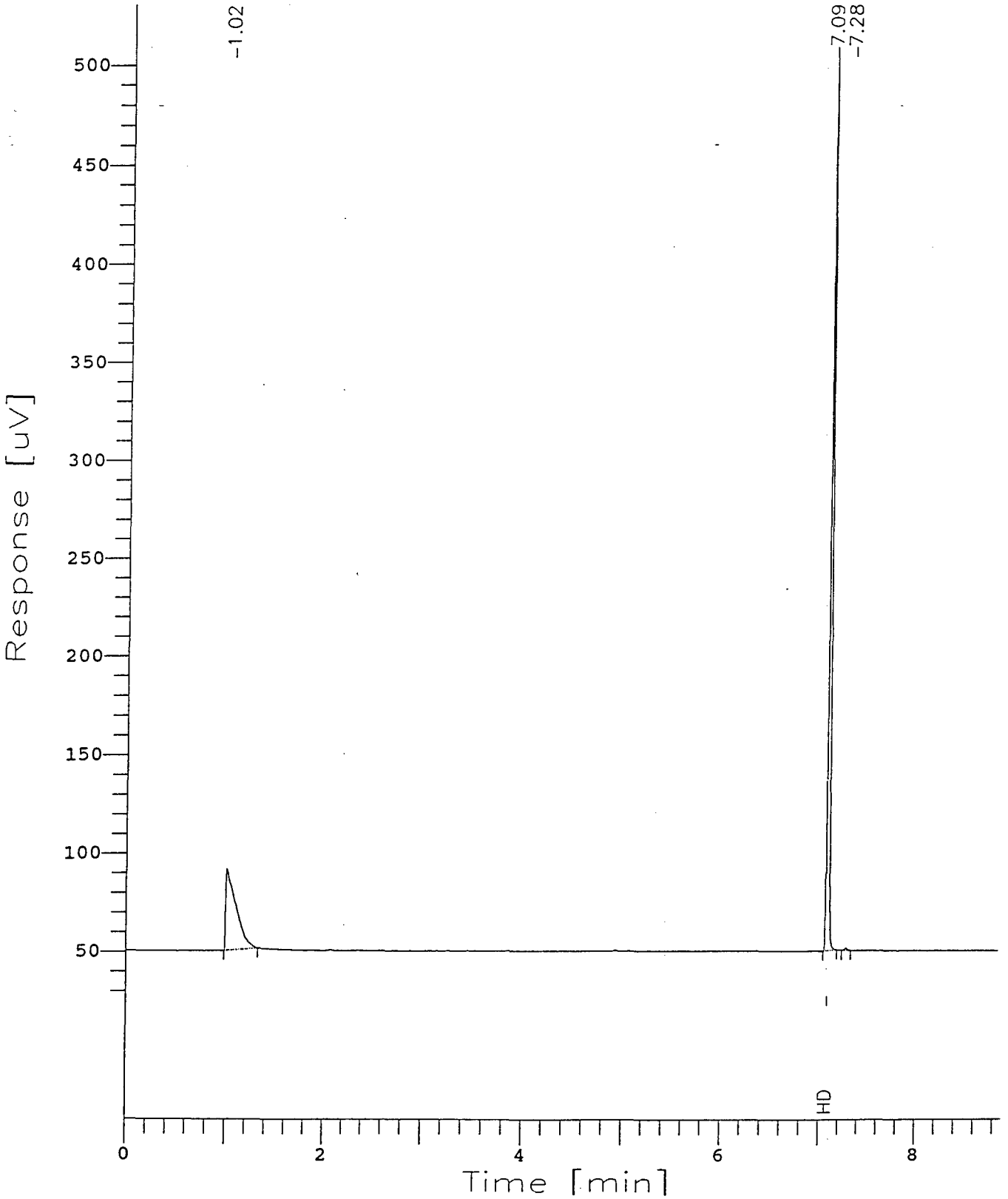

Figure 5. 4 µL HD on Fe_2O_3, Sample 2 After 6-Hour Extraction

Chromatogram

Sample Name : CONCAL 2.49ug/mL
FileName : C:\2700\GC\GC_R\VXEC008.raw
Method : E107VX
Start Time : 0.00 min End Time : 26.99 min
Scale Factor: 1.0 Plot Offset: 19 mV

Sample #: 4728-13-9 Page 1 of 1
Date : 5/11/97 02:16 PM
Time of Injection: 5/11/97 01:28 PM
Low Point : 18.98 mV High Point : 236.85 mV
Plot Scale: 217.9 mV

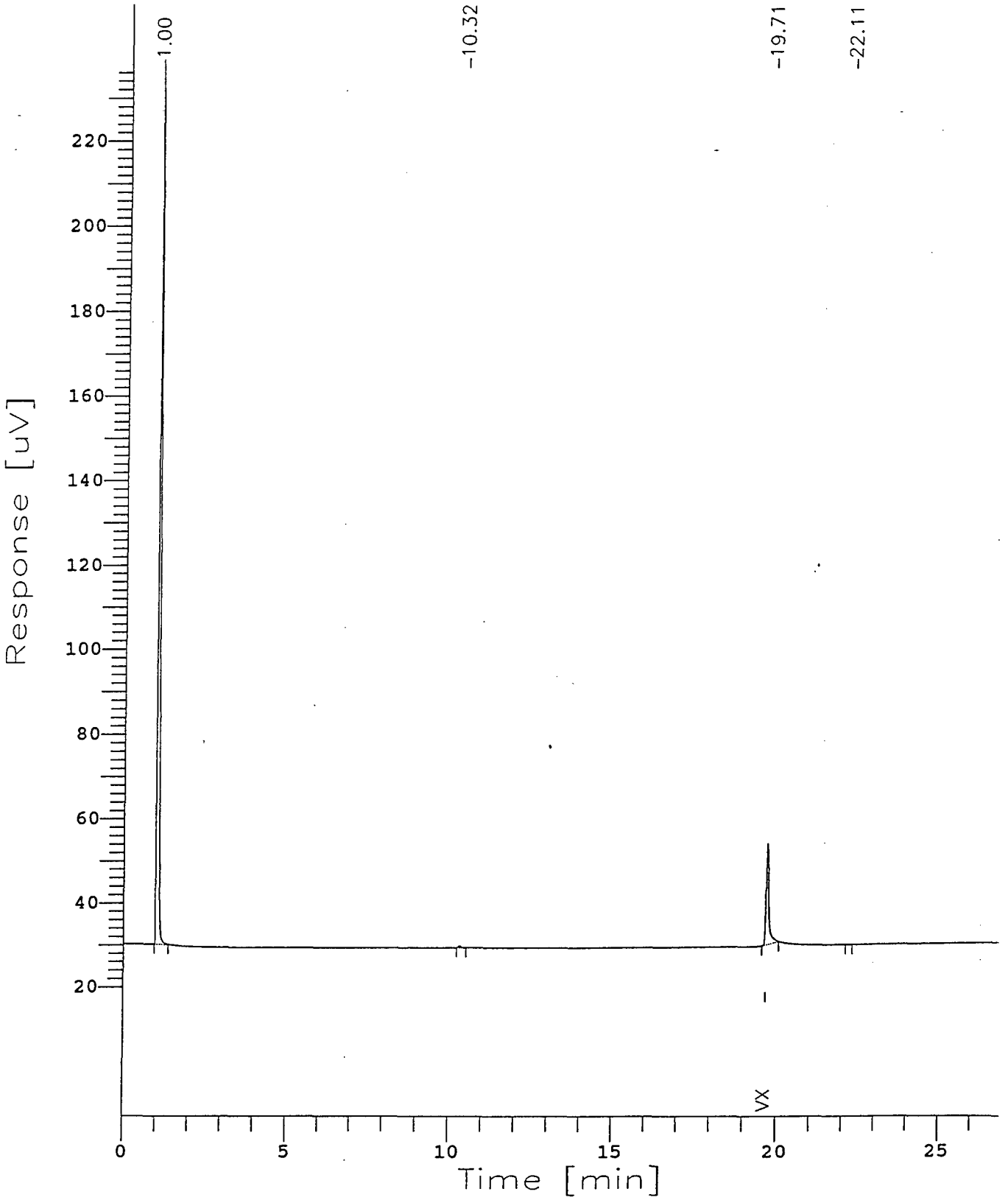

Figure 6. VX Standard (2.5 µg/mL)

Chromatogram

Sample Name : E127-1 2HR
FileName : c:\2700\gc\gc_r\VXEC013.raw
Method : E107VX.ins
Start Time : 0.00 min End Time : 26.99 min
Scale Factor: 1.0 Plot Offset: 19 mV

Sample #: MgO, SPK Page 1 of 1
Date : 5/12/97 05:15 PM
Time of Injection: 5/12/97 04:48 PM
Low Point : 19.45 mV High Point : 226.60 mV
Plot Scale: 207.1 mV

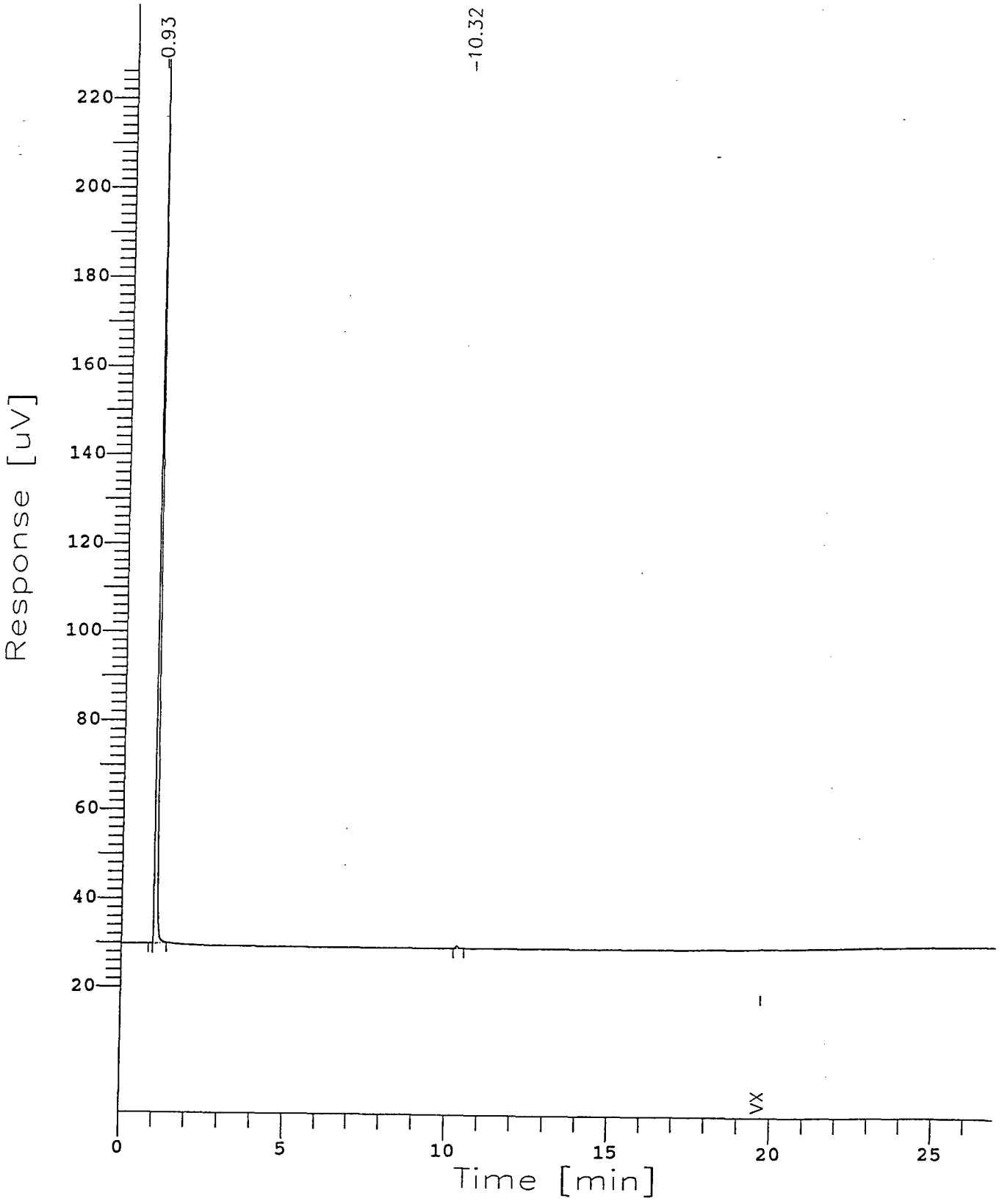

Figure 7. 4 µL VX on MgO After 2 Hours

Chromatogram

Sample Name : E287-2 2HR
FileName : c:\2700\gc\gc_r\E287008.raw
Method : E107VX.ins
Start Time : 0.00 min End Time : 26.99 min
Scale Factor: 1.0 Plot Offset: 18 mV

Sample #: MgO, SPK Page 1 of 1
Date : 5/28/97 04:57 PM
Time of Injection: 5/28/97 04:30 PM
Low Point : 17.92 mV High Point : 255.74 mV
Plot Scale: 237.8 mV

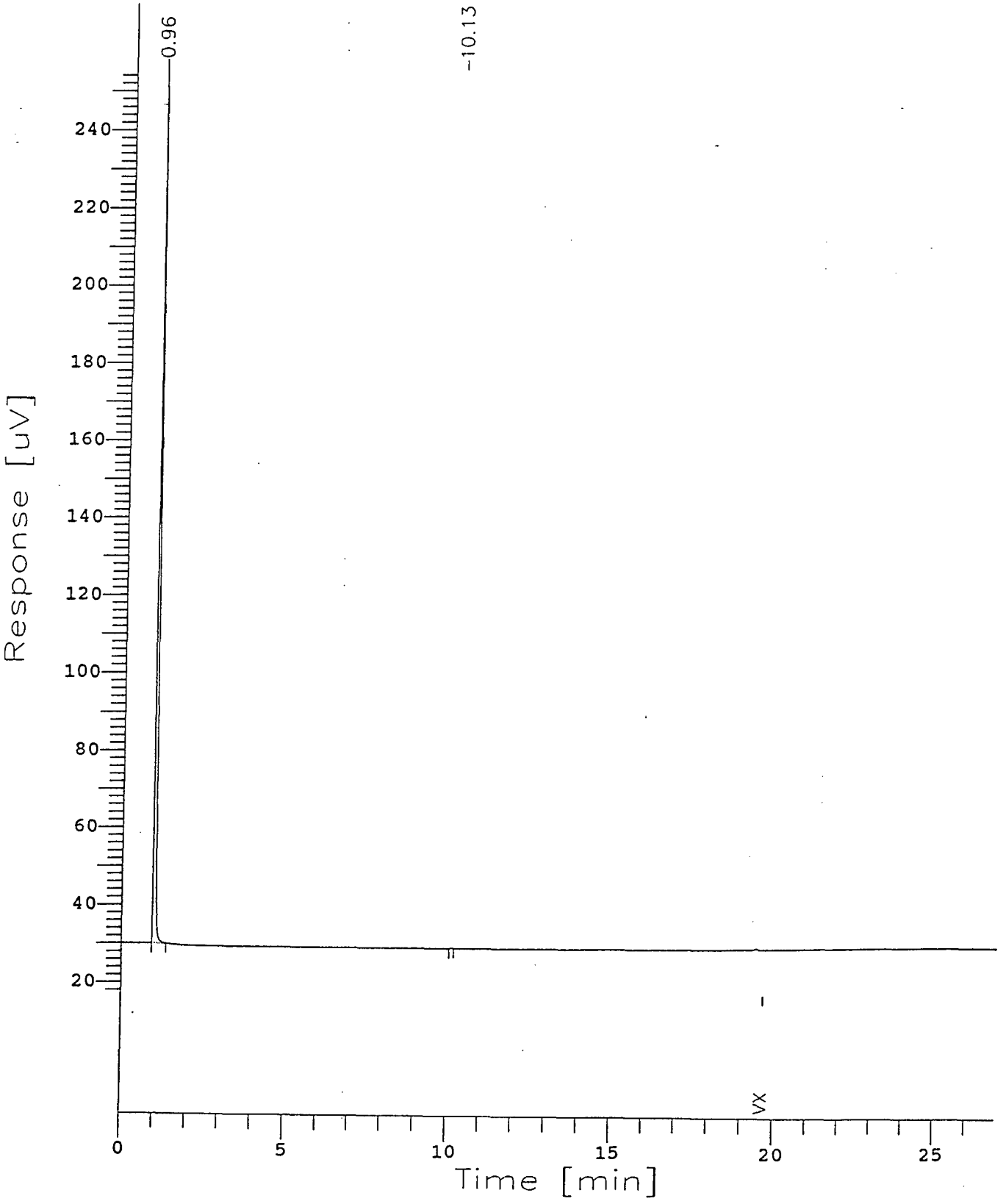

Figure 8. 20 µL of VX on MgO After 2 Hours

Chromatogram

Sample Name : E297-1 2HR
FileName : C:\2700\GC\GC_R\E297007.raw
Method : E107VX
Start Time : 0.00 min End Time : 26.99 min
Scale Factor: 1.0 Plot Offset: 19 mV

Sample #: FeO, SPK Page 1 of 1
Date : 5/30/97 01:56 PM
Time of Injection: 5/29/97 09:14 PM
Low Point : 18.86 mV High Point : 252.39 mV
Plot Scale: 233.5 mV

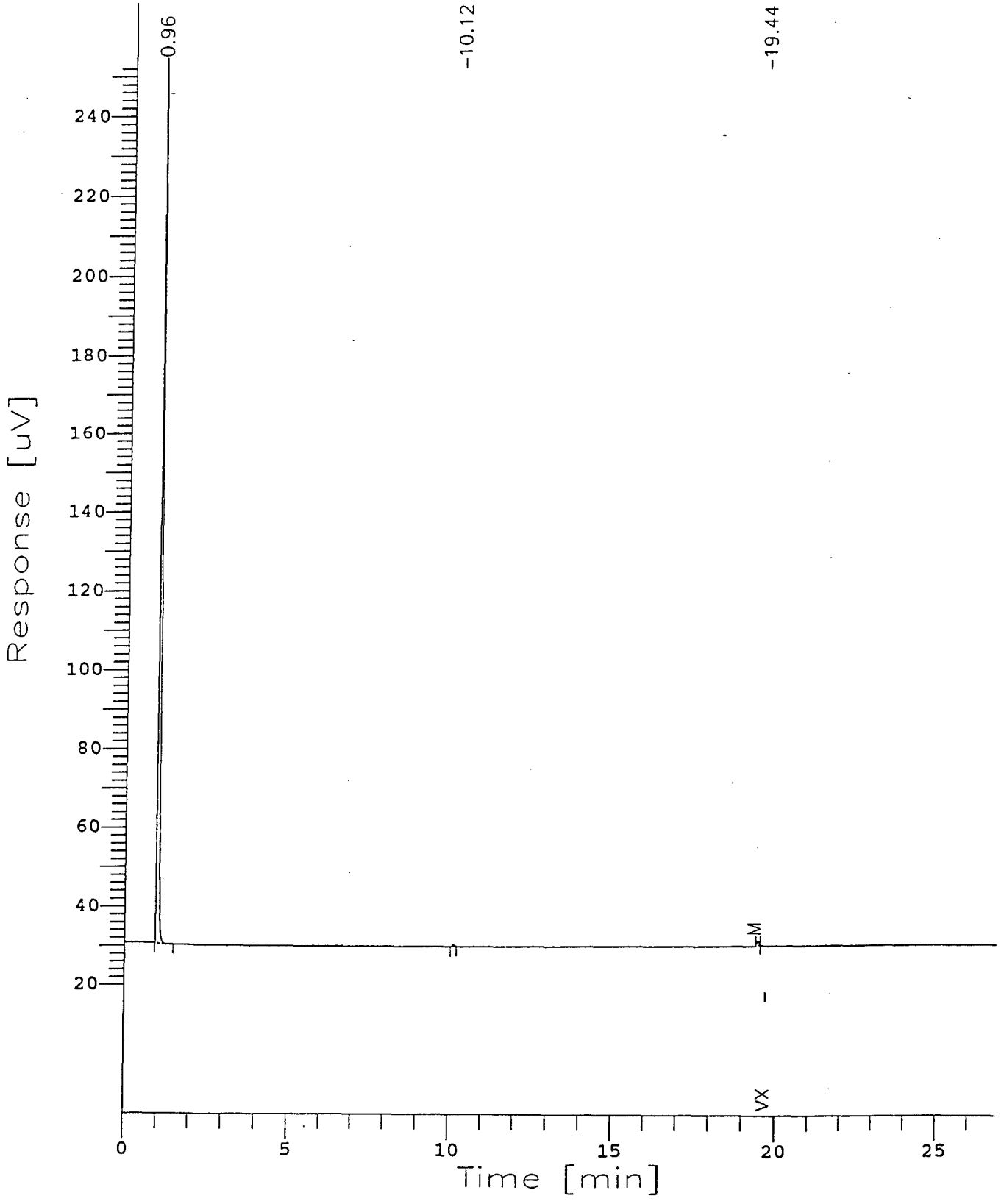

Figure 9. 4 µL of VX on Fe_2O_3 After 2 Hours

Chromatogram

Sample Name : E297-1 6HR
FileName : c:\2700\gc\gc_r\E297015.raw
Method : E107VX
Start Time : 0.00 min End Time : 26.99 min
Scale Factor: 1.0 Plot Offset: 19 mV

Sample #: FeO, SPK Page 1 of 1
Date : 5/30/97 09:14 AM
Time of Injection: 5/30/97 01:51 AM
Low Point : 18.64 mV High Point : 257.20 mV
Plot Scale: 238.6 mV

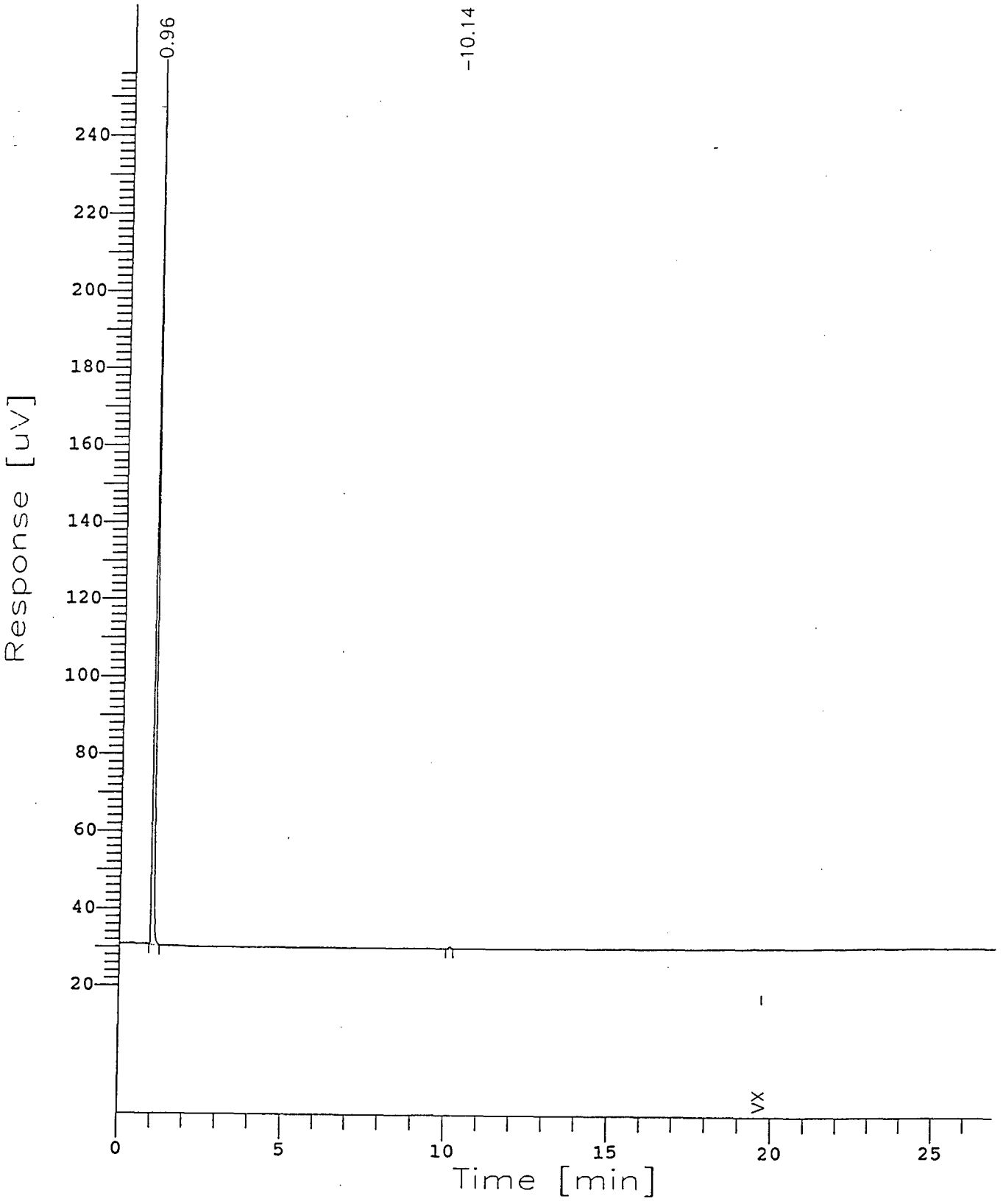

Figure 10. 4 µL of VX on Fe_2O_3 After 6 Hours

Chromatogram

Sample Name : E307-1 2HR
FileName : c:\2700\gc\gc_r\E307007.raw
Method : E107VX.ins
Start Time : 0.00 min End Time : 26.99 min
Scale Factor: 1.0 Plot Offset: 20 mV

Sample #: FeO, SPK Page 1 of 1
Date : 5/30/97 03:40 PM
Time of Injection: 5/30/97 03:12 PM
Low Point : 20.05 mV High Point : 230.57 mV
Plot Scale: 210.5 mV

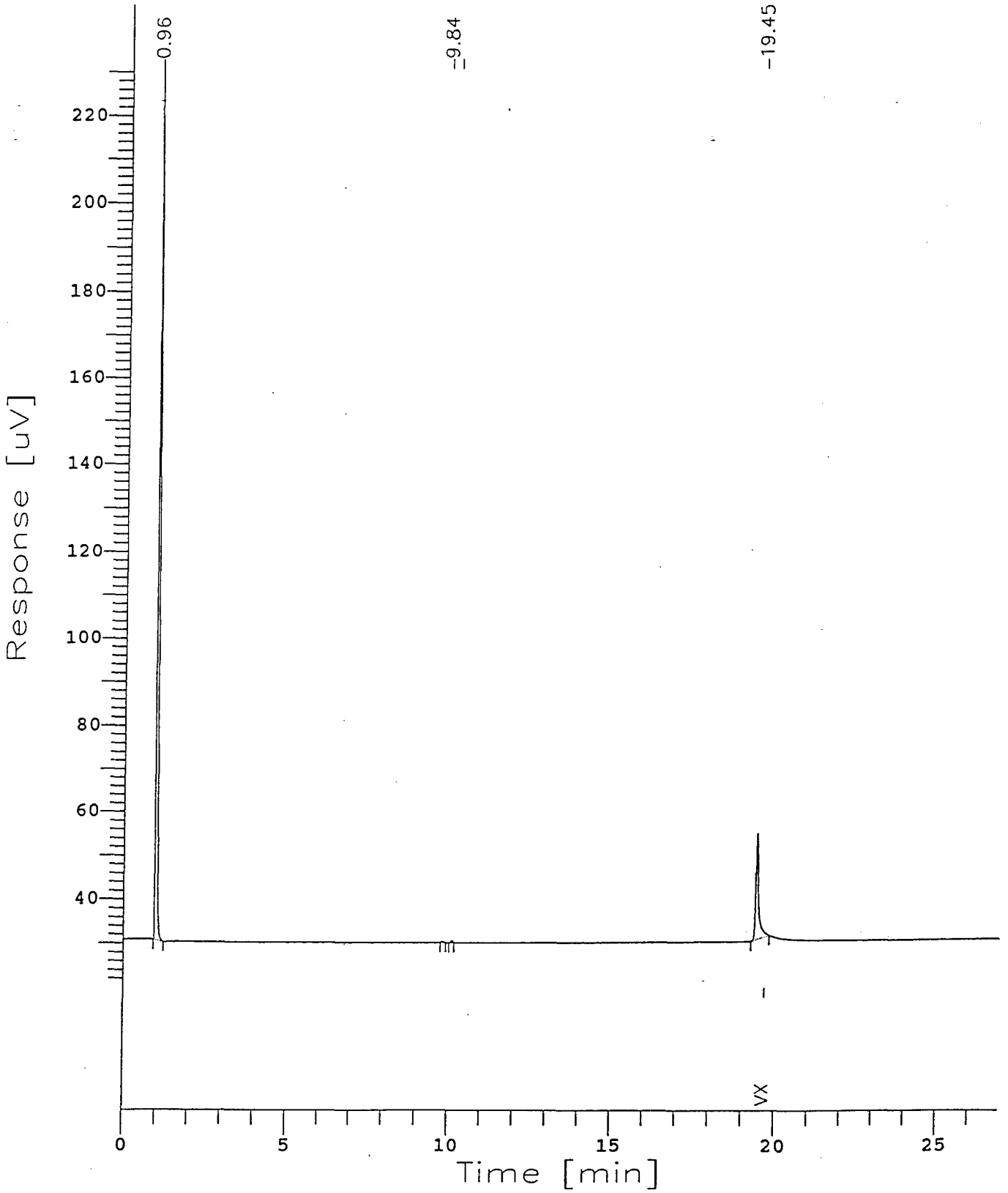

Figure 11. 20 µL of VX on Fe_2O_3, Sample 1 After 2 Hours

Chromatogram

Sample Name : E307-2 2HR
FileName : c:\2700\gc\gc_r\E307008.raw
Method : E107VX.ins
Start Time : 0.00 min End Time : 26.99 min
Scale Factor: 1.0 Plot Offset: 20 mV

Sample #: FeO, SPK Page 1 of 1
Date : 5/30/97 04:15 PM
Time of Injection: 5/30/97 03:48 PM
Low Point : 20.24 mV High Point : 227.72 mV
Plot Scale: 207.5 mV

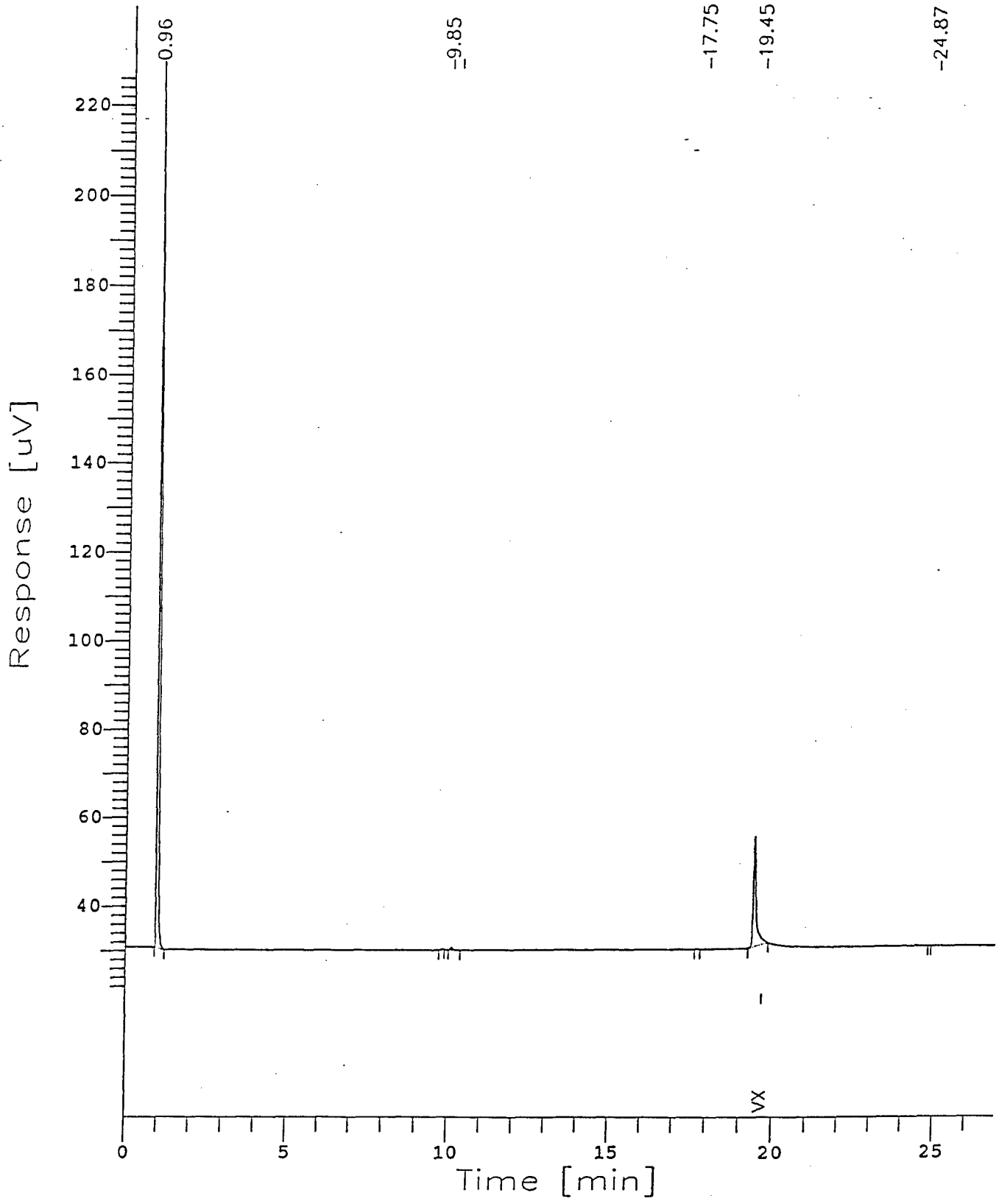

Figure 12. 20 µL of VX on Fe_2O_3, Sample 2 After 2 Hours

Chromatogram

Sample Name : E307-1 6HR
FileName : c:\2700\gc\gc_r\E307013.raw
Method : E107VX.ins
Start Time : 0.00 min End Time : 26.99 min
Scale Factor: 1.0 Plot Offset: 21 mV

Sample #: FeO, SPK Page 1 of 1
Date : 5/30/97 07:11 PM
Time of Injection: 5/30/97 06:44 PM
Low Point : 20.68 mV High Point : 219.88 mV
Plot Scale: 199.2 mV

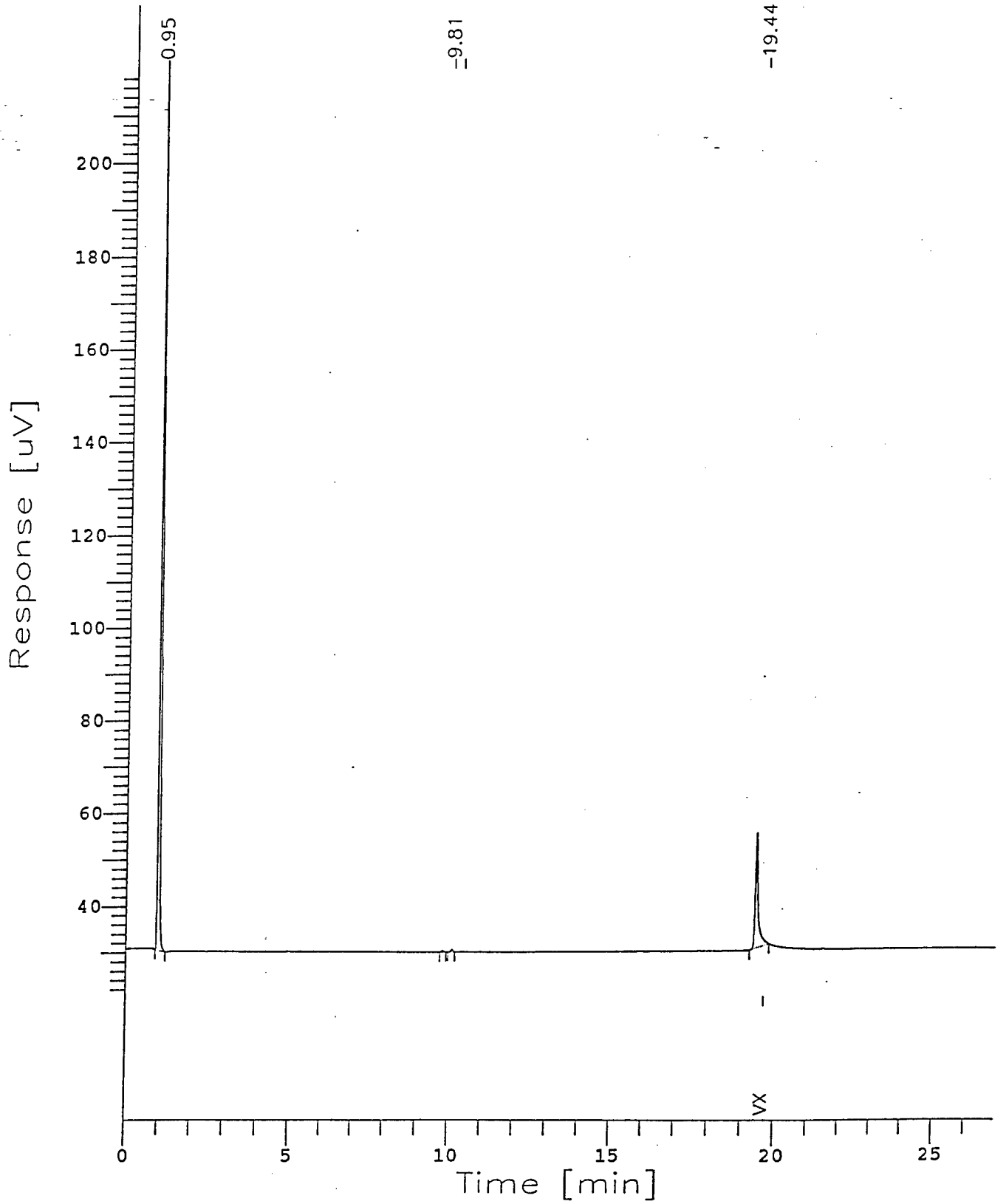

Figure 13. Figure 20 µL of VX on Fe_2O_3, Sample 1 After 6 Hours

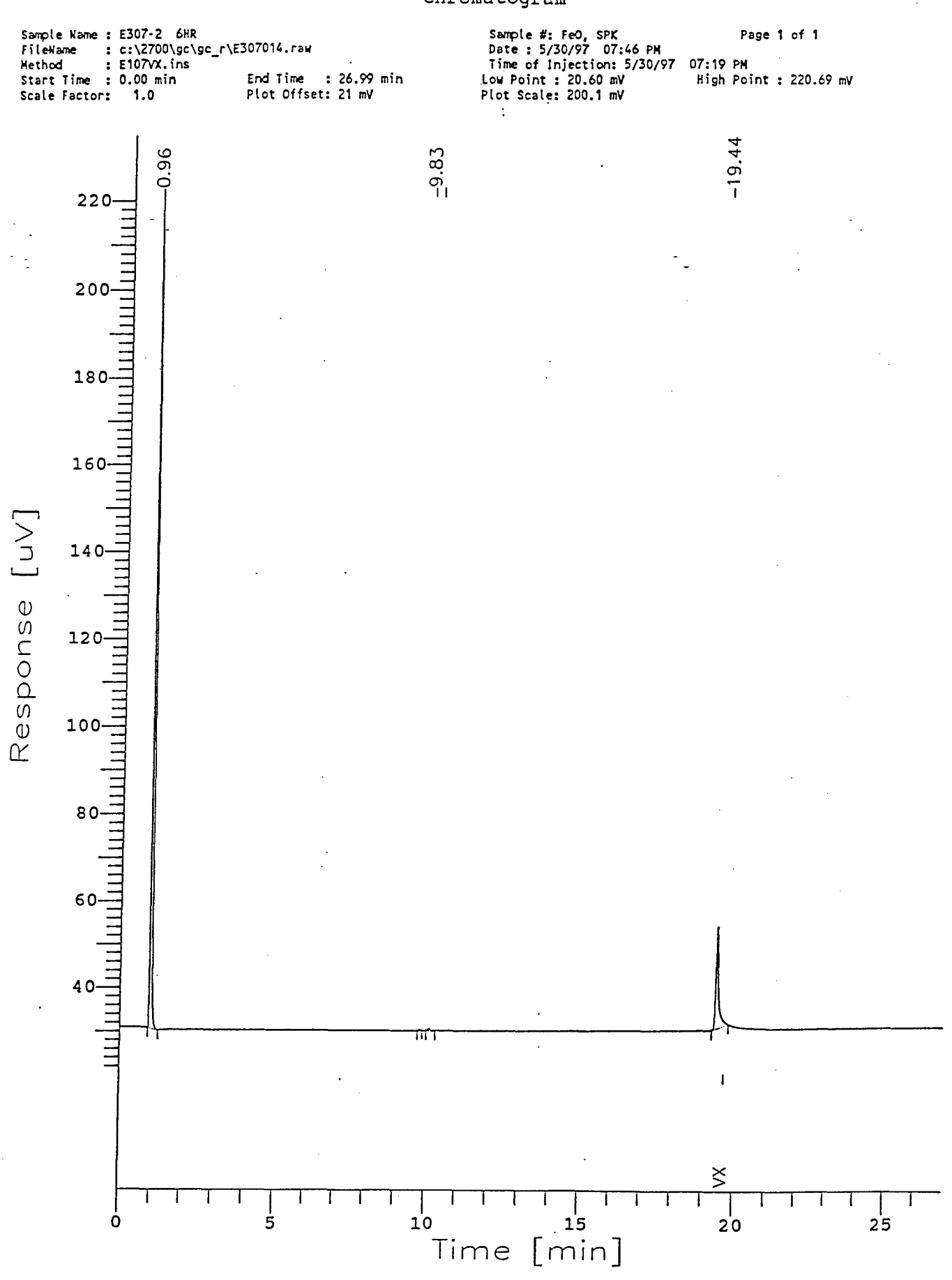

DAMD17-97-C-7016 **Figure 14. 20 µL of VX on Fe_2O_3, Sample 2 After 6 Hours** CBR Final Report

APPENDIX B

LIST OF TECHNICAL PERSONNEL

The following personnel received compensation during the Phase I Research effort:

Kenneth J. Klabunde, Principal Investigator

Olga Koper, Scientist

Slawomir Winecki, Scientist

APPENDIX C

LIST OF FIGURES

DEPARTMENT OF THE ARMY
US ARMY MEDICAL RESEARCH AND MATERIEL COMMAND
504 SCOTT STREET
FORT DETRICK, MARYLAND 21702-5012

REPLY TO
ATTENTION OF:

MCMR-RMI-S (70-1y) 4 Dec 02

MEMORANDUM FOR Administrator, Defense Technical Information Center (DTIC-OCA), 8725 John J. Kingman Road, Fort Belvoir, VA 22060-6218

SUBJECT: Request Change in Distribution Statement

1. The U.S. Army Medical Research and Materiel Command has reexamined the need for the limitation assigned to technical reports written for this Command. Request the limited distribution statement for the enclosed accession numbers be changed to "Approved for public release; distribution unlimited." These reports should be released to the National Technical Information Service.

2. Point of contact for this request is Ms. Kristin Morrow at DSN 343-7327 or by e-mail at Kristin.Morrow@det.amedd.army.mil.

FOR THE COMMANDER:

Encl

PHYLIS M. RINEHART
Deputy Chief of Staff for
Information Management

ADB218773
ADB223531
ADB230017
ADB223528
ADB231930
ADB226038
ADB224296
ADB228898
ADB216077
ADB218568
ADB216713
ADB216627
ADB215717
ADB218709
ADB216942
ADB216071
ADB215736
ADB216715
ADB215485
ADB215487
ADB220304
ADB215719
ADB216072
ADB222892
ADB215914
ADB222994
ADB216066
ADB217309
ADB216726
ADB216947
ADB227451
ADB229334
ADB228982
ADB227216
ADB224877
ADB224876
ADB227768
ADB228161
ADB229442
ADB230946
ADB230047
ADB225895
ADB229467
ADB224342
ADB230950
ADB227185
ADB231856
ADB229914
ADB229497
ADB230947
ADB282209
ADB270846
ADB282266
ADB262442
ADB256670